Geochemistry Geophysics Geosystems G3
AN ELECTRONIC JOURNAL OF THE EARTH SCIENCES
Published by AGU and the Geochemical Society

Article
Volume 9, Number 3
5 March 2008
Q03003, doi:10.1029/2007GC001699
ISSN: 1525-2027

Fault rotation and core complex formation: Significant processes in seafloor formation at slow-spreading mid-ocean ridges (Mid-Atlantic Ridge, 13°–15°N)

Deborah K. Smith
Geology and Geophysics Department, Woods Hole Oceanographic Institution, Woods Hole, Massachusetts 02543, USA (dsmith@whoi.edu)

Javier Escartín
Groupe de Geosciences Marines, CNRS - IPGP, 75252 Paris, France

Hans Schouten
Geology and Geophysics Department, Woods Hole Oceanographic Institution, Woods Hole, Massachusetts 02543, USA

Johnson R. Cann
School of Earth and Environment, University of Leeds, Leeds LS2 9JT, UK

[1] The region of the Mid-Atlantic Ridge (MAR) between the Fifteen-Twenty and Marathon fracture zones displays the topographic characteristics of prevalent and vigorous tectonic extension. Normal faults show large amounts of rotation, dome-shaped corrugated detachment surfaces (core complexes) intersect the seafloor at the edge of the inner valley floor, and extinct core complexes cover the seafloor off-axis. We have identified 45 potential core complexes in this region whose locations are scattered everywhere along two segments (13° and 15°N segments). Steep outward-facing slopes suggest that the footwalls of many of the normal faults in these two segments have rotated by more than 30°. The rotation occurs very close to the ridge axis (as much as 20° within 5 km of the volcanic axis) and is complete by ~1 My, producing distinctive linear ridges with roughly symmetrical slopes. This morphology is very different from linear abyssal hill faults formed at the 14°N magmatic segment, which display a smaller amount of rotation (typically <15°). We suggest that the severe rotation of faults is diagnostic of a region undergoing large amounts of tectonic extension on single faults. If faults are long-lived, a dome-shaped corrugated surface develops in front of the ridges and lower crustal and upper mantle rocks are exposed to form a core complex. A single ridge segment can have several active core complexes, some less than 25 km apart that are separated by swales. We present two models for multiple core complex formation: a continuous model in which a single detachment surface extends along axis to include all of the core complexes and swales, and a discontinuous model in which local detachment faults form the core complexes and magmatic spreading forms the intervening swales. Either model can explain the observed morphology.

Components: 11,653 words, 14 figures.

Keywords: slow-spreading ridges; detachment faulting; ocean core complex; fault rotation.

Index Terms: 3035 Marine Geology and Geophysics: Midocean ridge processes; 3045 Marine Geology and Geophysics: Seafloor morphology, geology, and geophysics; 3075 Marine Geology and Geophysics: Submarine tectonics and volcanism.

Received 22 May 2007; **Revised** 11 November 2007; **Accepted** 27 November 2007; **Published** 5 March 2008.

Smith, D. K., J. Escartín, H. Schouten, and J. R. Cann (2008), Fault rotation and core complex formation: Significant processes in seafloor formation at slow-spreading mid-ocean ridges (Mid-Atlantic Ridge, 13°–15°N), *Geochem. Geophys. Geosyst.*, *9*, Q03003, doi:10.1029/2007GC001699.

1. Introduction

[2] Ocean core complexes are massifs in which lower crustal and upper mantle rocks are exposed at the seafloor [*Blackman et al.*, 1998; *Cann et al.*, 1997; *Dick et al.*, 1981; *Tucholke et al.*, 1998]. They form at slow- and intermediate-spreading mid-ocean ridges through slip on detachment faults that initiated close to the spreading axis [*Blackman et al.*, 1998; *Escartín et al.*, 2003a; *MacLeod et al.*, 2002; *Searle et al.*, 2003; *Tucholke et al.*, 1998]. The exposed detachment surfaces commonly show corrugations that run parallel to the spreading direction.

[3] While most ocean core complexes have been observed near the ends of segments they also occur away from them [*Blackman et al.*, 1998; *Cann et al.*, 1997; *Cannat et al.*, 1995, 2006; *Christie et al.*, 1998; *deMartin et al.*, 2007; e.g., *Escartín and Cannat*, 1999; *Escartín et al.*, 2003a; *MacLeod et al.*, 2002; *Ohara et al.*, 2001; *Searle et al.*, 2003; *Tivey et al.*, 2003]. In two recent studies, it has been found that core complexes can occur anywhere along segments at the Southwest Indian Ridge [*Cannat et al.*, 2006] and the Mid-Atlantic Ridge (MAR) [*Smith et al.*, 2006] prompting a reexamination of the controls on core complex formation. In this paper we expand the study of *Smith et al.* [2006], which identified several active core complexes between 13°40′N and 12°50′N at the MAR, to a much broader region centered on the ridge axis between the Fifteen-Twenty (15°20′N) and Marathon (12°14′N) fracture zones (Figure 1). The multitude of core complexes found in this region allow us to identify the various stages and morphologies associated with slip on detachment faults and to present two models of core complex formation.

2. Study Area

[4] Our study area in the equatorial Atlantic has had a complex tectonic history associated with movement of the North American-South American-African (NA-SA-AF) triple junction and the opening of the Atlantic Ocean [e.g., *Bonatti*, 1996; *Jones*, 1987; *Klitgord and Schouten*, 1986; *LePichon and Fox*, 1971; *Uchupi*, 1989]. The NA-SA-AF triple junction may have migrated from near 10°N to the 14°–16°N region between 72.5 and 35.5 Ma [*Müller and Smith*, 1993], and there may still be some motion between the NA and SA plates [e.g., *DeMets et al.*, 1994; *Dixon and Mao*, 1997; *Müller and Smith*, 1993; *Sella et al.*, 2002]. The plate boundary is commonly assumed to be near the Fifteen-Twenty fracture zone, but it is not clearly marked by seismicity or unambiguous tectonic features. Today, the positions of both the NA-SA-AF and the NA-SA-Caribbean triple junctions remain under debate [e.g., *Escartín et al.*, 2003b].

[5] The ridge axis near the Fifteen-Twenty fracture zone has been the focus of several studies, which include geophysical surveys [*Escartín and Cannat*, 1999; *Fujiwara et al.*, 2003], dredge and submersible sampling [*Cannat et al.*, 1992; *Cannat and Casey*, 1995; *Cannat et al.*, 1997; *Lagabrielle et al.*, 1998], and drilling [*Escartín et al.*, 2003a; *Garces and Gee*, 2007; *Kelemen et al.*, 2004; *MacLeod et al.*, 2002; *Schroeder et al.*, 2007]. These studies have been motivated in large part by the discovery of the Logachev high-temperature vent field hosted in peridotites near 14°45′N [e.g., *Bogdanov et al.*, 1995; *Sudarikov and Roumiantsev*, 2000] and the multitude of exposures of lower crustal and upper mantle rocks in the axial zones both north and south of the fracture zone.

[6] Only a few geophysical studies have been conducted south of 14°N [e.g., *Collette et al.*, 1974]. Sparse sampling along the axis between ~14°N and the Marathon fracture zone [e.g., *Sarda and Graham*, 1990] recovered basalts, that gave geochemical data showing an anomaly [*Dosso et al.*, 1991, 1993] indicating a possible hot-spot origin [e.g., *Javoy and Pineau*, 1991; *Sarda and Graham*, 1990]. The Ashadze hydrothermal vent field, also hosted in peridotites, was discovered near 12°55′N [*Beltnenev et al.*, 2003; *Sudarikov et al.*, 2001] and more recent work has developed from that discovery. The Ashadze vent field and the area around it were one of the targets of both the "Serpentine" cruise of the N/O *Porquois Pas*? (Y. Fouquet, P. I.) and the cruise of the Russian R/V *Professor Logachev* in the Spring of 2007.

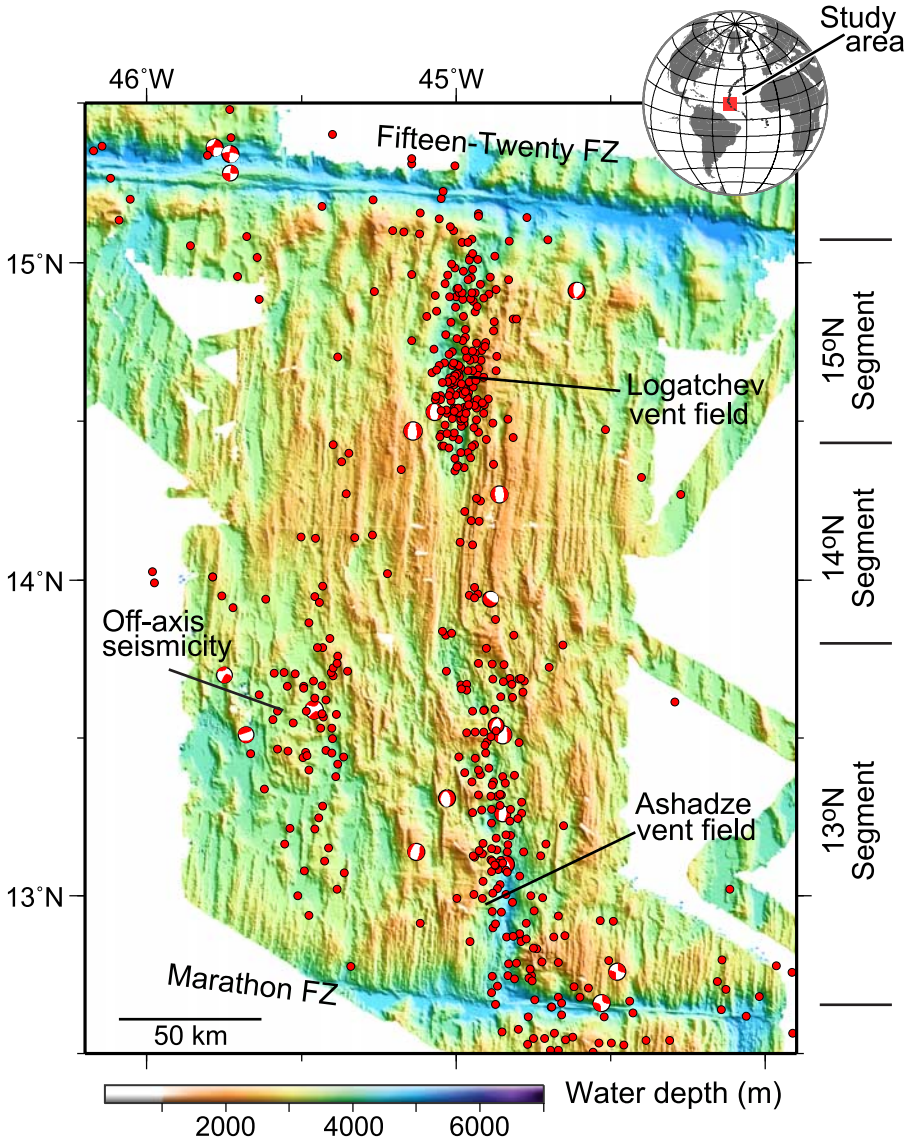

Figure 1. Multibeam bathymetry data between Fifteen Twenty and Marathon fracture zones. Data north of 14°10′N are from *Fujiwara et al.* [2003] and *Escartín and Cannat* [1999]. The ridge axis is divided into 3 'segments' based on morphology. Beach balls: locations of teleseismically recorded events between 1976–2007 from the Harvard Centroid-Moment Tensor Catalog. Red dots: locations of hydroacoustically-recorded seismic events [*Escartín et al.*, 2003b; *Smith et al.*, 2003]. Known hydrothermal vent fields are marked.

Additional geophysical and geological studies, motivated by the results of *Smith et al.* [2006] were conducted in Spring 2007 onboard R/V *James Clark Ross* (R. C. Searle, P. I.). Apart from a magnetic profile on the east flank of our survey area collected during the Serpentine cruise and provided by M. Cannat, the present paper has not benefited from the results of these cruises.

3. Data

[7] A geophysical survey of the region of the MAR between 14°10′N and the Marathon fracture zone [*Smith et al.*, 2006] collected SeaBeam bathymetry and sea-surface magnetic and gravity data (Figures 2a–2c). Survey tracks were spaced at ~9 km to provide 100% bathymetric coverage (Figure 2d). As the initial E-W tracks resulted in a poor magnetic signal due to instrument malfunction, we conducted most of the survey along NW-SE tracks, allowing us to improve the magnetometer's signal strength. We have combined our survey data with those of *Fujiwara et al.* [2003] and *Escartín and Cannat* [1999] to extend our study region north to the Fifteen-Twenty fracture zone.

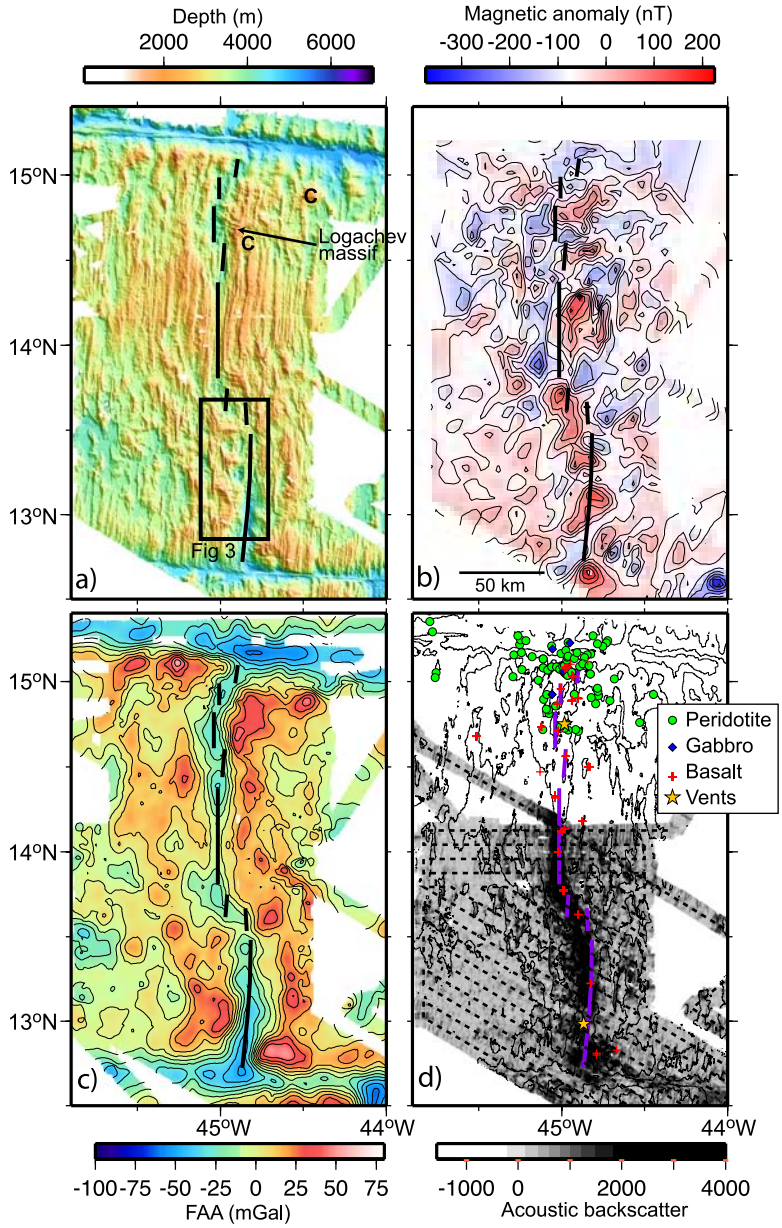

Figure 2. Data for the region between Fifteen Twenty and Marathon fracture zones from this study combined with those from *Fujiwara et al.* [2003] and *Escartín and Cannat* [1999]. Ridge axis is shown as a thick, segmented line. (a) Multibeam bathymetry data. The Logachev massif is marked. The area outlined is shown in greater detail in Figure 3. 'C': locations of core complexes identified by *Fujiwara et al.* [2003]. (b) Magnetic anomaly data. (c) Free air gravity data. (d) Acoustic backscatter plotted with dark indicating high amplitude returns and white low amplitude. Dashed lines: tracklines for the data collected by *Smith et al.* [2006]. Gold stars: hydrothermal vent fields hosted in ultramafic rocks. Green dots: locations where peridotites have been sampled. Blue diamonds: locations where gabbros have been sampled. Red plus: locations where basalts have been sampled.

[8] The multibeam bathymetry and associated acoustic backscatter data were collected using the SeaBeam 2100 system and extend from ~14°10′N to south of the Marathon fracture zone. Off-axis coverage extends ~100 km on the west flank, and ~30 km on the east flank. Figure 2a displays the bathymetry and Figure 2d the acoustic backscatter derived from the SeaBeam 2100 system. High amplitude backscatter (black) represents regions of low sediment cover or scarps. Low amplitude backscatter (white) is generally associated with significant sediment cover.

[9] Magnetic total field data were obtained along the ship tracks at a sampling interval of 1 s using an IXSEA magnetometer. The total field data were decimated to a 1-minute interval. Magnetic anomaly was obtained by removing the International Geomagnetic Reference Field (IGRF) [*IAGA*, 1996] updated in 2005 from the total field data. The resulting magnetic anomaly data show variations between tracks. We investigated whether the variations were associated with changes in ship heading but there was no clear association. We did observe some evidence of diurnal variations in the magnetic field, but did not correct for it because the associated amplitude variation was within the standard deviation of the data. The magnetic anomaly data were combined with those of *Fujiwara et al.* [2003] and evenly gridded with a 3 km spacing between data points (Figure 2b) using the Generic Mapping Tool (GMT [*Wessel and Smith*, 1991]) software.

[10] Gravity data were collected along the ship tracks using a NAVO BGM-3 gravimeter at a sampling interval of 1 s. The raw gravity data were filtered using the GMT 5-minute robust Gaussian filter [*Wessel and Smith*, 1998]. An 8-minute median filter was applied to the filtered output, and the data were decimated to a 1-minute interval. After correcting for Eötvos effects, sensor drift, and dc shifts using the absolute gravity ties obtained at the beginning and end of the cruise, the free-air gravity anomaly was calculated by subtracting the IAGA 1980 theoretical gravity formula from the corrected data. The free-air gravity anomaly data were merged with those of *Fujiwara et al.* [2003] and from individual ship tracks from the NGDC catalog (http://www.ngdc.noaa.gov). Data were split in linear tracks and shifted to minimize differences with the along-track satellite-derived gravity, thus reducing cross-over errors. The combined along-track free-air data were gridded in GMT at 3 km data spacing to produce the map displayed in Figure 2c.

[11] From 1999 to 2005 an autonomous hydrophone array in the North Atlantic [*Smith et al.*, 2002] recorded the hydroacoustic energy from thousands of earthquakes whose locations are much better located (a few kilometers) than those detected teleseismically [e.g., *Bohnenstiehl et al.*, 2002]. The hydrophone array monitored the ridge axis between 15° and 35°N, and recorded events with magnitudes greater than ~2.5 [e.g., *Bohnenstiehl et al.*, 2002; *Williams et al.*, 2006]. The hydrophone data and more information about them can be obtained at http://autochart.pmel.noaa.gov:1776/autochart/GetPosit. Because of the nature of hydroacoustically-recorded data we have no information on earthquake depth or focal mechanisms. Nonetheless, patterns of seismicity are recognized along the axis from these data and have been interpreted in terms of geologic processes [e.g., *Dziak et al.*, 2004; *Smith et al.*, 2002, 2003]. We have used these data to examine the distribution of seismicity in the spreading segments examined in this work (Figure 1).

4. Ridge Axis Characteristics and Segmentation

[12] In order to refer to the different sections of the ridge axis between the Fifteen-Twenty and Marathon fracture zones we have divided the axis into 3 'segments' based on morphology and seismicity patterns. *Smith et al.* [2006] have previously referred to the 13° and 14° segments as topographically blocky and volcanic, respectively, but did not provide details on their characteristics. These are given below.

4.1. The 15°N Segment

[13] This segment extends from the Fifteen-Twenty fracture zone to 14°20′N. *Fujiwara et al.* [2003] divided this region into multiple segments, but we link them here into a single unit. Depths along the axis range from 3600 m to 4300 m. Deep basins occur regularly along the axis. The flanks of the 15°N segment are described by *Fujiwara et al.* [2003] as topographically irregular and blocky and likely generated by irregular fault patterns. Two large core complexes were identified on the eastern flank [*Escartín and Cannat*, 1999; *Fujiwara et al.*, 2003] (Figure 2a). Hydroacoustically-recorded seismicity indicates that the axis of the 15°N segment is seismically active along its length (Figure 1). A relatively high number of seismic events are located close to the Logachev massif on the east side of the axis at 14°45′N. Seismic events extend to the southern tip of the 15°N segment (Figure 1) and may be associated with propagation of the axis to the south.

4.2. The 14°N Segment

[14] The axis of the 14°N segment extends between ~14°20′N and ~13°45′N. The flanks are characterized by long abyssal hills that run parallel to the spreading center, show clear volcanic mor-

phology, and have steep scarps facing the spreading axis [e.g., *Escartín and Cannat*, 1999; *Fujiwara et al.*, 2003; *Schroeder et al.*, 2007]. A continuous zone of high acoustic backscatter (Figure 2d) defines the spreading axis. The amplitude of the backscatter decreases significantly on crust outside of the first bounding fault of the inner valley floor suggesting that the axis is continually repaved by lavas at a rate sufficient to prevent significant sediment accumulation. The bathymetry along the axis is deep at the ends of the segment and shallows to ~2900 m near the center. Hydrophone-recorded events are scarce in the 14°N segment. Overall, the morphology of the 14°N segment is typical of many of the segments of the northern MAR that are considered magmatically robust [e.g., *Sempéré et al.*, 1993; *Thibaud et al.*, 1998].

4.3. The 13°N Segment

[15] The axis of the 13°N segment extends south from ~13°45′N to the Marathon fracture zone. The flanks of the 13°N segment are topographically irregular and blocky similar to those of the 15°N segment. Depths along the axis are variable. The northern half of the axis has an average depth of ~3300 m; in the southern half the axis deepens significantly to an average of ~4600 m. The zone of high acoustic backscatter is significantly broader in the 13°N segment than in the 14°N segment. Between 13°30′N and 13°20′N the width of the zone of high amplitudes increases to include the massifs identified as active core complexes [*Smith et al.*, 2006] suggesting that the exhumed footwalls are not heavily sedimented. A region ~15 km long, centered near 13°N on the axis has low backscatter amplitudes, indicating that significant sediment has accumulated in this region, and that volcanic repaving has been sparse.

[16] Seismic activity is relatively high in the 13°N segment. It is broadly scattered along the axis, and thought to be associated with slipping on detachment faults [*Smith et al.*, 2006]. An unusual zone of hydrophone-recorded seismicity occurs about 70 km west of the axis (~5.5 My old crust), and trends parallel to the ridge for ~100 km [*Escartín et al.*, 2003b] (Figure 1). At the axis available focal mechanisms from teleseismic earthquakes show extension directions that are consistent with NA-AF or SA-AF plate spreading (~E-W). In contrast, focal mechanisms from earthquakes located in the off-axis strip show extension directions consistent with NA-SA spreading (~NNW-SSE) [*Escartín et al.*, 2003b]. Whether this seismicity is a manifestation of the NA-SA plate boundary remains unknown and will require further information to determine its origin.

5. Identifying Core Complexes

5.1. Near-Axis Features of *Smith et al.* [2006]

[17] *Smith et al.* [2006] showed that the seafloor on the western flank of the 13°N segment is dominated by linear ridges typically tens of kilometers long with slopes dipping both toward and away from the spreading axis (Figure 3). The outward-facing slopes of the ridges they described, dipping ~15–20°, have a tilted hummocky morphology typical of the axial valley floor of the MAR.

[18] Confirmation of the tilting comes from the top of a small cratered volcanic cone mapped on the outward-facing slope of a ridge at 13°30′N, 45°15′W, which has been rotated 16° away from the spreading axis during the evolution of the ridge. From these observations, *Smith et al.* [2006] concluded that the linear ridges are the surface expression of rotated normal faults, and that the outward-facing slopes are back-tilted sections of the originally subhorizontal median valley floor. The steep (>40°) inward-facing normal faults of the linear ridges typically grade into flatter and smoother seafloor, largely corrugated parallel to the spreading direction. The corrugated surfaces were interpreted as the exposed fault planes that cap oceanic core complexes that have been rotated to shallow angles during extension exhuming lower crustal and upper mantle rocks.

[19] The detailed morphology of the core complexes identified by *Smith et al.* [2006] is shown in Figure 3a. The dome-shaped corrugated surfaces labeled 1 and 2 on Figures 3a and 3b dip at an angle of about 15° where they meet the median valley floor along a curved line 2–5 km west of the volcanic spreading axis. These were identified as active detachment faults. A larger and apparently compound core complex extends for 30–40 km parallel to the axis between ~13°15′N and 12°56′N and includes complexes '3', '4' and '5'. A corrugated surface is present over a large part of the complex '4' (corrugations are difficult to distinguish at the map scale of Figure 3.) The Ashadze peridotite-hosted hydrothermal vent field [*Beltnenev et al.*, 2003] is located on its southeastern edge (star in Figure 3a). Between the core

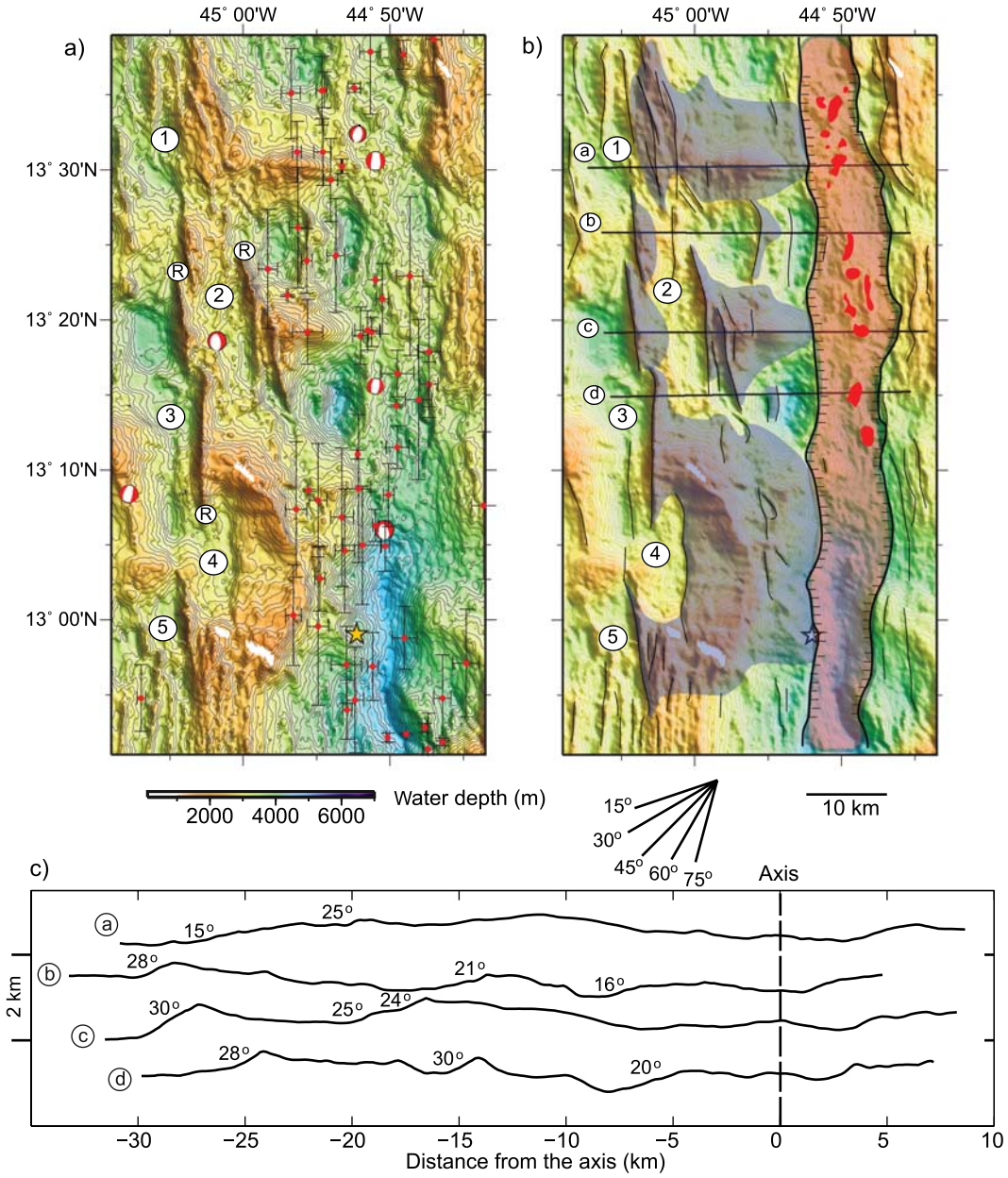

Figure 3. (a) Bathymetry for the box shown in Figure 2a, contoured at 100-m intervals. Numbered features: core complexes identified by *Smith et al.* [2006]. R: linear ridges interpreted as marking rotated blocks of seafloor. Beach balls: locations of teleseismically recorded events between 1976–2007 from the Harvard Centroid-Moment Tensor Catalog. Red dots: locations of hydroacoustically-recorded seismic events with 1σ error bars. Gold star: Ashadze vent field. (b) Gray shading: features identified as core complexes and rotated blocks. Light red shading: inner valley floor. Note that the intersection of the footwalls of the core complexes with the seafloor marks the edge of the inner valley floor. Black line with inward-facing hachures: bounding fault of the valley floor. Red areas: interpreted volcanic centers. Black lines: inward- and outward-facing scarps, some of which mark linear ridges. (c) Profiles for the E-W lines in (b) shown with no vertical exaggeration. Values of outward-facing slopes are shown.

complexes are areas of seafloor characterized by linear ridges backed by deep basins (Figures 3b and 3c). *Smith et al.* [2006] identified these as places where faults had rotated outwards and new detachment footwalls are emerging from below the seafloor.

[20] The features described by *Smith et al.* [2006] are the starting point for extending our study to the broader region between the Fifteen-Twenty and Marathon fracture zones. We also use near-bottom data collected at 16°30′N to add to our argument

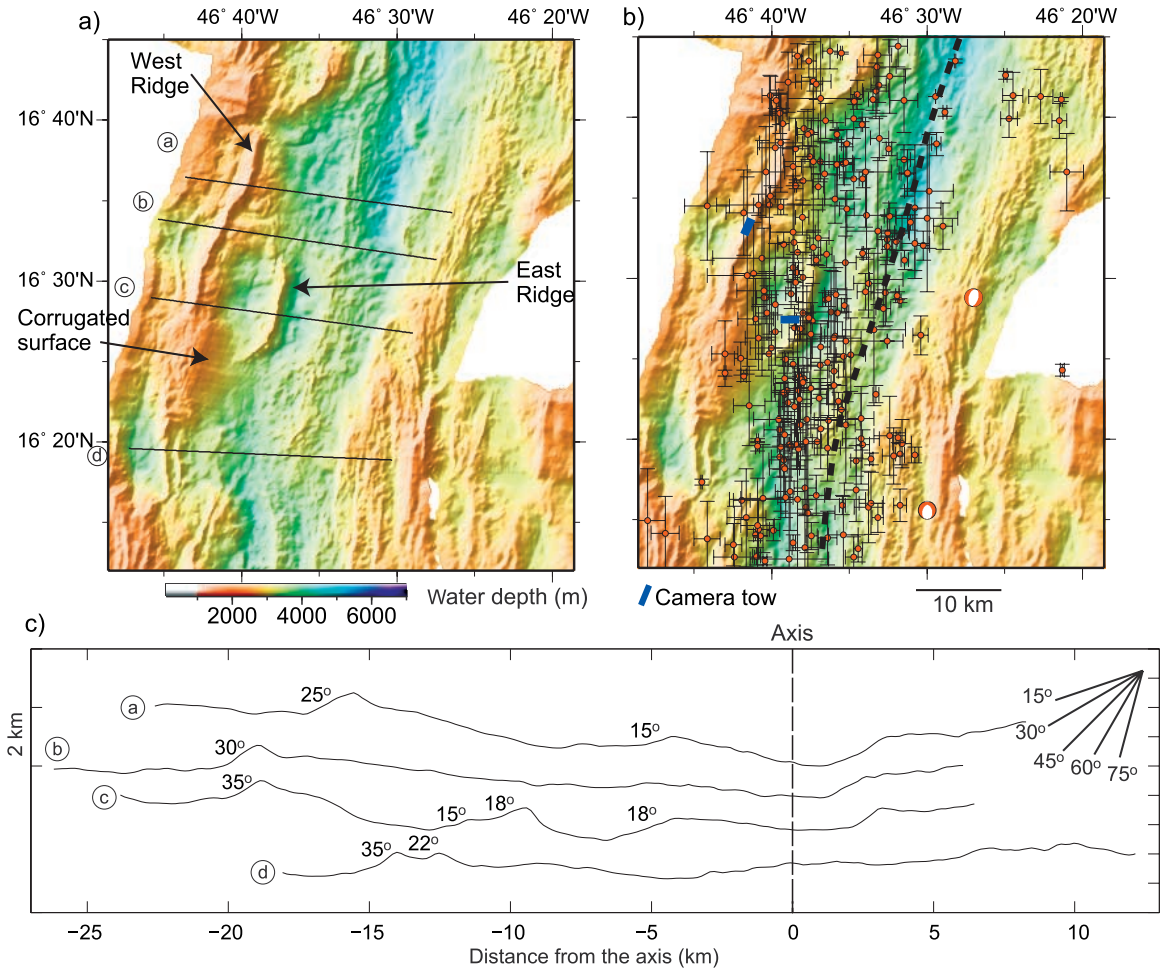

Figure 4. (a) Bathymetry of the MAR axis near 16°30′N. Two distinctive linear ridges are observed in this region – labeled East and West ridges. A corrugated core complex is marked. Circles with letters and black lines: locations of profiles shown in (c). (b) Bathymetry map as in (a). Black dashed line: spreading axis. Beach balls: locations of teleseismically recorded events between 1976–2007 from the Harvard Centroid-Moment Tensor Catalog. Red dots: locations of hydroacoustically-recorded seismic events with 1σ error bars. Blue lines: location of camera tows conducted in 2001 on R/V *Atlantis*, Cruise 4-4 (D. Smith, chief scientist). (c) Bathymetric profiles over the linear ridges plotted as a function of distance from the spreading axis. There is no vertical exaggeration. The dips of the outward-facing slopes are shown.

that the outward-facing slopes are rotated sections of originally flat-lying volcanic seafloor.

5.2. Near-Axis Features at 16°30′N Along the MAR

[21] In 2001 on R/V *Atlantis*, Cruise 4-4 (D. Smith, chief scientist), the morphology of the axial zone at 16°30′N (Figure 4a), 300 km north of our main study area, was investigated. The axis at 16°30′N has an above average rate of hydroacoustically-recorded seismicity (Figure 4b) [*Smith et al.*, 2003], and distinctive linear ridges and corrugated surfaces extend along the western flank of the axis. Cross-axis profiles over the linear ridges (Figure 4c) show that the dips of the outward-facing slopes are similar to those documented in the 13°N segment (Figure 3c). Camera tows near the tops of what we refer to as East and West ridges at 16°30′N (Figures 4a and 4b) show that both ridges expose pillow basalts variably covered by sediment.

[22] Photographs from the 18° outward-facing slope of East Ridge are displayed in Figure 5. The start of the tow (not shown on Figure 5a) dipped briefly over the 30° inward-facing eastern edge of the ridge and showed steep scarps cutting pillow lavas. On the outward-facing slopes more or less equant pillows are observed (Figures 5b and 5c). Pillows that erupt onto slopes of this magnitude are typically elongate down slope, so we infer that the pillows were emplaced on subhorizontal surfaces

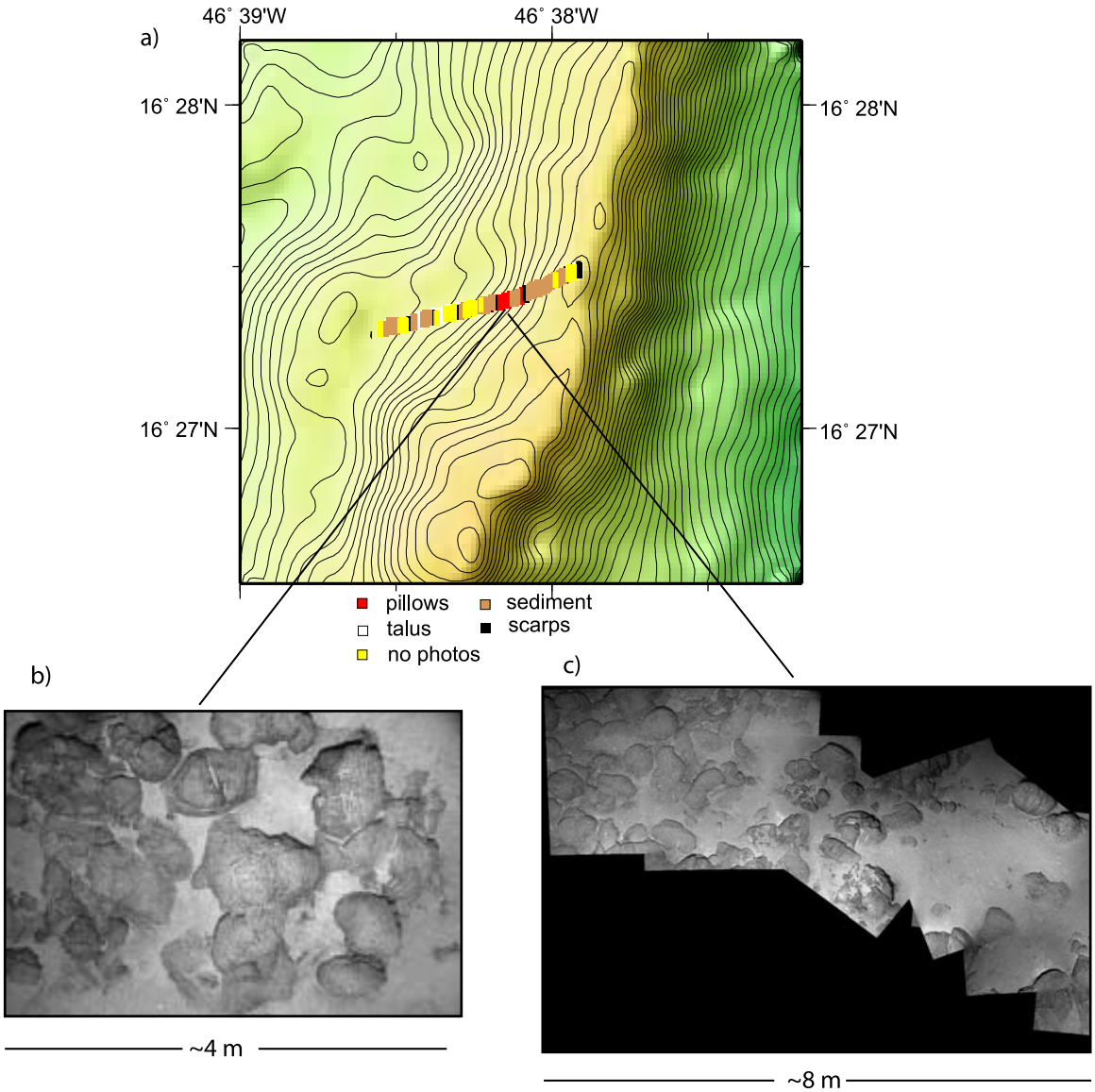

Figure 5. (a) Detailed bathymetry map for the region of the camera tow on East ridge shown in Figure 4b. Depths are contoured at 25-m intervals. Colored boxes: interpretation of the photographs along the tow, which traversed the outward-facing slope of East ridge. (b) Photograph and (c) Photomosaic of pillows observed midway along the camera tow (generated by R. Garcia, U. Girona, Spain). Note the pillows are equant in shape. Pillows erupted onto slopes of this magnitude are typically elongate downslope suggesting that these pillows were formed on subhorizontal surfaces and subsequently rotated outward.

that had been subsequently rotated outward. (No images from the outward-facing slope of West Ridge were obtained.)

[23] Equant pillows also have been observed on the outward-facing slopes of linear ridges in other regions at the MAR. They are found on a linear ridge associated with the Kane megamullion (C. Williams, personal communication), an extinct core complex south of the Kane fracture zone [*Tucholke et al.*, 1996]. In addition, *Tucholke et al.* [2001] reported pillow basalts on the outward-facing slope of a linear ridge associated with a core complex at 26°40′N east of the axis. These observations help to support our hypothesis that linear ridges are normal faults that have rotated during extension resulting in backtilted volcanic seafloor of the median valley floor.

5.3. Outward-Facing Slopes and Fault Rotation

[24] The outward-facing slopes of the profiles shown in Figures 3c and 4c indicate that significant

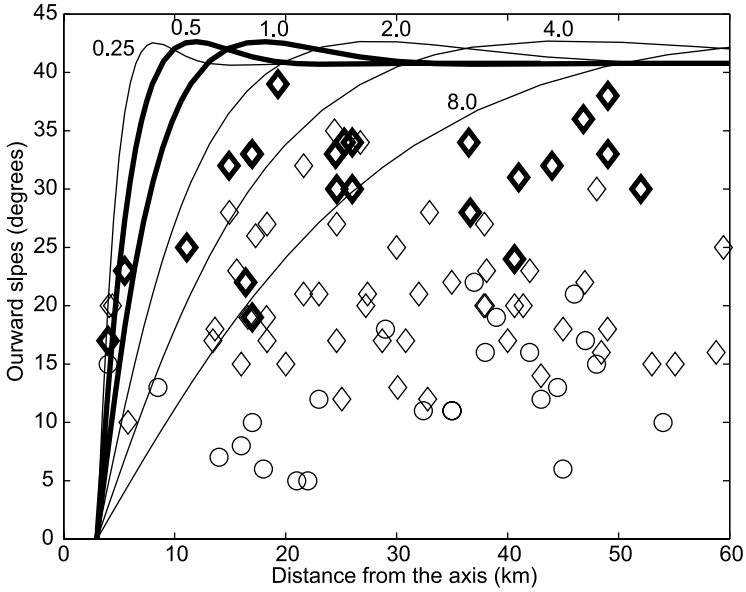

Figure 6. Measures of 115 outward-facing slopes are plotted against distance from the axis. Diamonds: slopes from the 13°N and 15°N segments; Circles: slopes from the 14°N segment. The outward-facing slopes in the 14°N segment are consistently low (12° ± 5°). In the 13°N and 15°N segments slopes frequently exceed 30°. Bold symbols: outward-facing slopes of linear ridges where the sum of inward and outward slopes is >45° implying that when the outward slopes are rotated back to an original horizontal orientation, the inward slopes would have dipped more than 45° toward the axis. Curves: the flexural rotation of a 60° normal fault for different values of Te (effective elastic thickness of the lithosphere) assuming that the fault initiates at ∼3 km from the axis. Bold curves: best-fitting envelope to the data points (Te = 0.5–1 km).

fault rotation (up to 20°) can occur very close to the axis (within 5 km); fault rotations of up to 35° are observed 15 km from the axis. To obtain a better understanding of fault extension and rotation (and ultimately core complex formation) within our study area, we measured the inward- and outward-facing slopes of ∼70 isolated linear ridges and ∼45 ridges that back core complexes between the Fifteen-Twenty and Marathon fracture zone. Measured outward-facing slopes are plotted against distance from the axis in Figure 6 (diamonds: 13°N and 15°N segments; circles: 14°N segment). The outward-facing slopes in the 14°N segment are consistently low (12° ± 5°). In contrast, those in the 13°N and 15°N segments frequently exceed 30°. If the outward-facing slopes were originally subhorizontal seafloor cut by a normal fault as argued in the previous section, and mass-wasting has not significantly modified their geometry, then as much as 20° of fault rotation can occur within 5 km of the volcanic axis (Figures 3c, 4c, and 6). An additional 10°–15° of rotation may occur within 10–15 km from the axis, so that by ∼1 My (12.5 km from the axis) most of the rotation on all faults is complete.

[25] The bold symbols in Figure 6 represent the outward slopes of linear ridges where the sum of inward and outward slopes is greater than 45°, which means that when the outward slopes are rotated back to an original horizontal orientation, the inward slopes would dip at more than 45° toward the axis, consistent with an origin as steep normal faults.

[26] Figure 6 also shows the flexural rotation of a 60° normal fault for different values of Te (effective elastic thickness). We assume that the fault initiates at ∼3 km from the axis and extends to the base of the crust at 6 km depth. The curves in Figure 6 thus represent the maximum possible rotation for a given Te. The curves in bold for Te = 0.5 and Te = 1 km are the best-fitting envelopes to the data.

[27] We suggest that the severe rotation of faults in the 13°N and 15°N segments indicates that a region is undergoing large amounts of tectonic extension on single faults. If faults are long-lived (large extension), dome-shaped corrugated surfaces may develop and lower crustal and upper mantle rocks may become exposed. We use these ideas to identify core complexes within our study region.

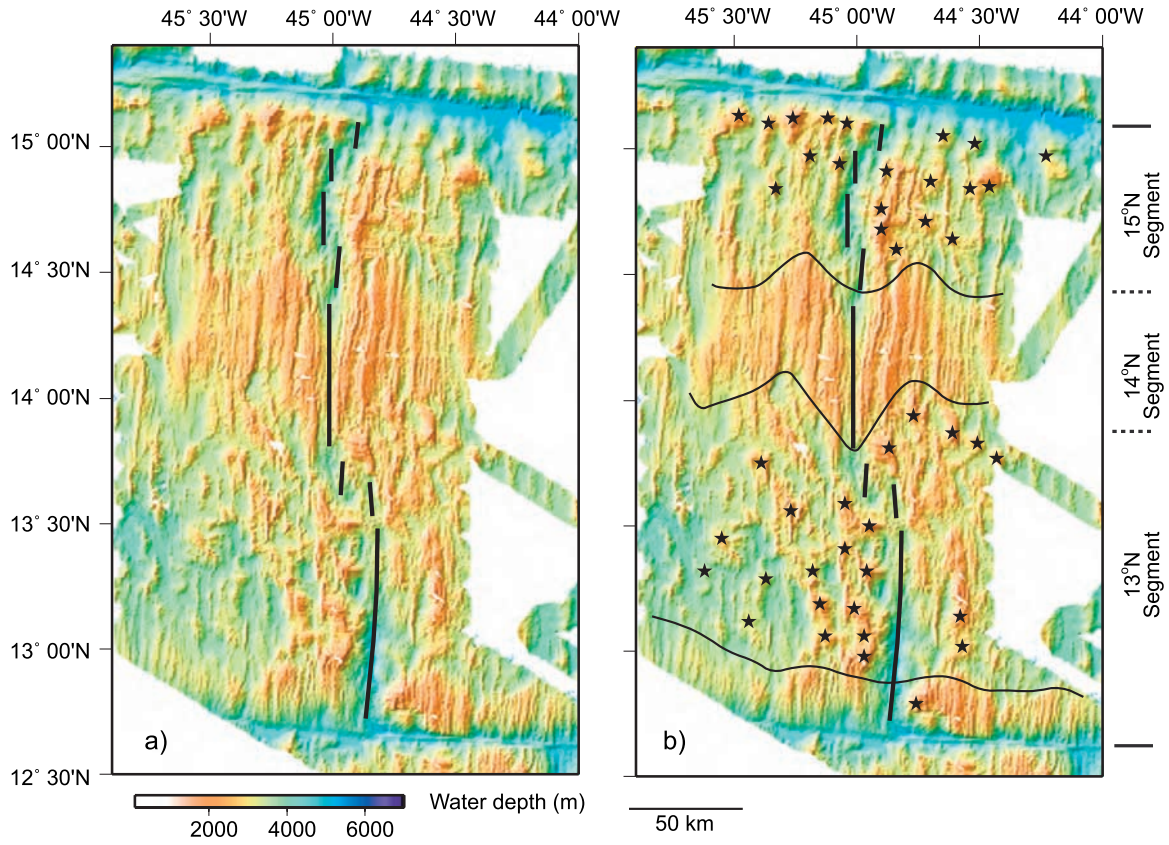

Figure 7. (a) Bathymetry between the Fifteen-Twenty and Marathon fracture zones. Black line: spreading axis. (b) Bathymetry map as in (a). Black stars: core complexes identified in this study. Light black lines: boundaries of the 14°N segment and in the south the boundary between detachment fault dominated terrain and volcanic terrain in the 13°N segment based on bathymetry and a slope map derived from the bathymetry at a spatial scale of 450 m.

5.4. Core Complexes Between the Fifteen-Twenty and Marathon Fracture Zones

[28] The core complexes we identified have several diagnostic features. They are all backed by distinctive outward-facing slopes ranging between 15° and 35°. The outward-facing slopes are the backs of linear ridges, which grade into flatter surfaces towards the axis. Multiple outward-facing slopes may be associated with a single core complex and we infer that they represent a succession of rotated normal faults that root into a single detachment fault. Core complexes are elevated compared to the surrounding seafloor. Corrugations may develop on the exhumed footwall. Examples of the 45 core complexes that we identified within our study region (Figure 7) are shown in Figures 8 and 9. The TAG core complex is shown in Figure 8c for comparison.

[29] Core complexes are primarily observed within the west flank of the 13°N segment and the east flank of the 15°N segment (Figure 7). The west flank of the 13°N segment has been dominated by core complex formation for 100 km of spreading (~8–9 My, assuming spreading has been symmetrical at ~12 mm/yr half rate). On the less-extensively mapped east flank of the 13°N segment we identify a series of core complexes that have formed at the northeastern boundary of the segment. In addition, two core complexes are identified in the southern part of the segment, and one adjacent to the Marathon fracture zone. The east flank of the 15°N segment has been dominated by core complex formation for at least the last 5 My (using the ages given by *Fujiwara et al.* [2003]). On the west flank of the 15°N segment, core complex massifs are primarily observed adjacent to the Fifteen-Twenty transform.

6. Magnetization and Gravity

[30] In the following sections we examine the geophysical field data to understand the controls

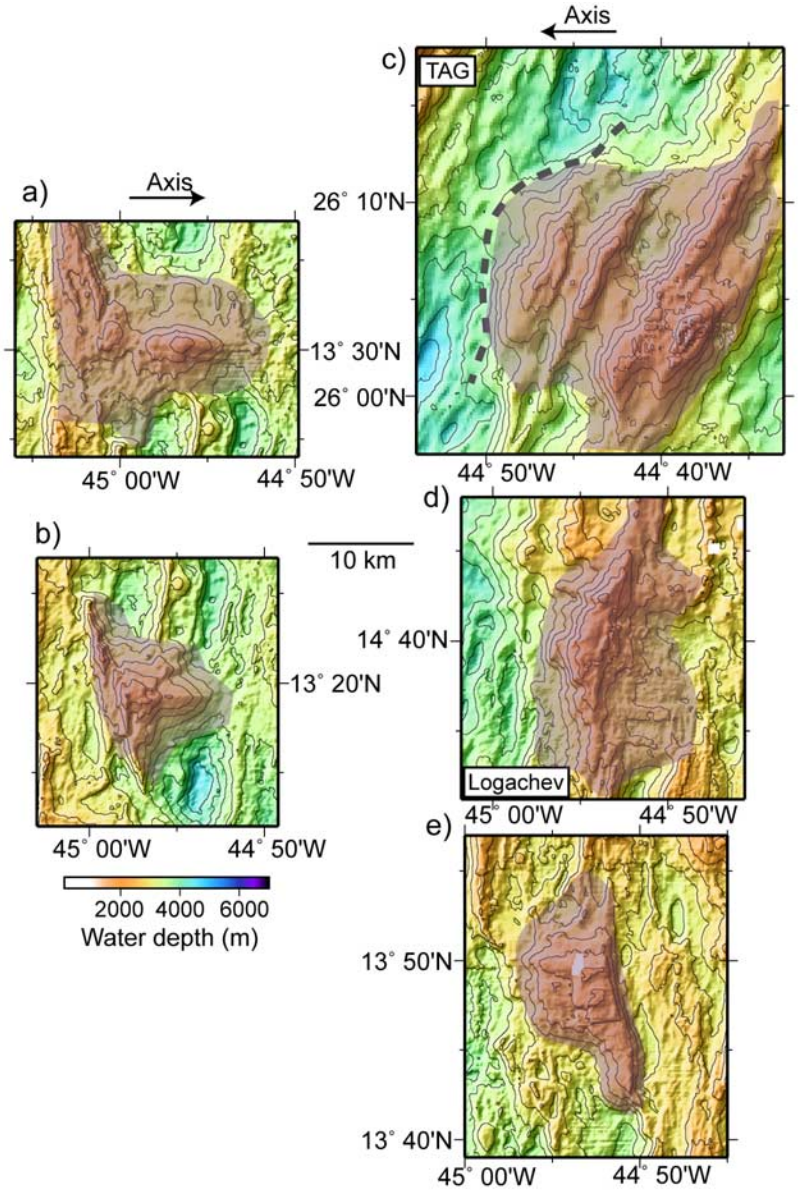

Figure 8. Bathymetry maps contoured at 250-m intervals of 5 core complexes bordering the axis. Maps are all plotted at the same scale. Shading: interpretation of the core complex massifs. (a) and (b) Core complexes shown in Figure 3. (c) TAG core complex at 26°N, bathymetry from *Canales et al.* [2007]. Dashed line: outline of the zone of epicenters from the microseismicity beneath the spreading center from *deMartin et al.* [2007]. Note the 3 linear ridges that make up the overall massif east of the ridge axis. We have identified corrugations between the ridges suggesting that detachment faulting has been occurring on the east flank of the TAG segment for at least the last 2 My instead of <0.5 My as suggested by *Tivey et al.* [2003]. (d) Area of the Logachev hydrothermal vent field and massif. The corrugated surface south of 14°40′N and east of the Logachev massif was identified by *Fujiwara et al.* [2003] as a core complex. (e) Core complex on the east side of the 13°N segment at its northern end.

on the formation of core complexes between the Fifteen-Twenty and Marathon fracture zones.

6.1. Crustal Magnetization

[31] Crustal magnetization was calculated for the region between the Fifteen-Twenty and Marathon fracture zones correcting for seafloor topography and removing skewness associated with the low latitudes of our study. We used the *Parker and Huestis* [1974] Fourier inversion procedure. The inversion was performed on the gridded magnetic anomaly data (grid spacing at 3 km) assuming a

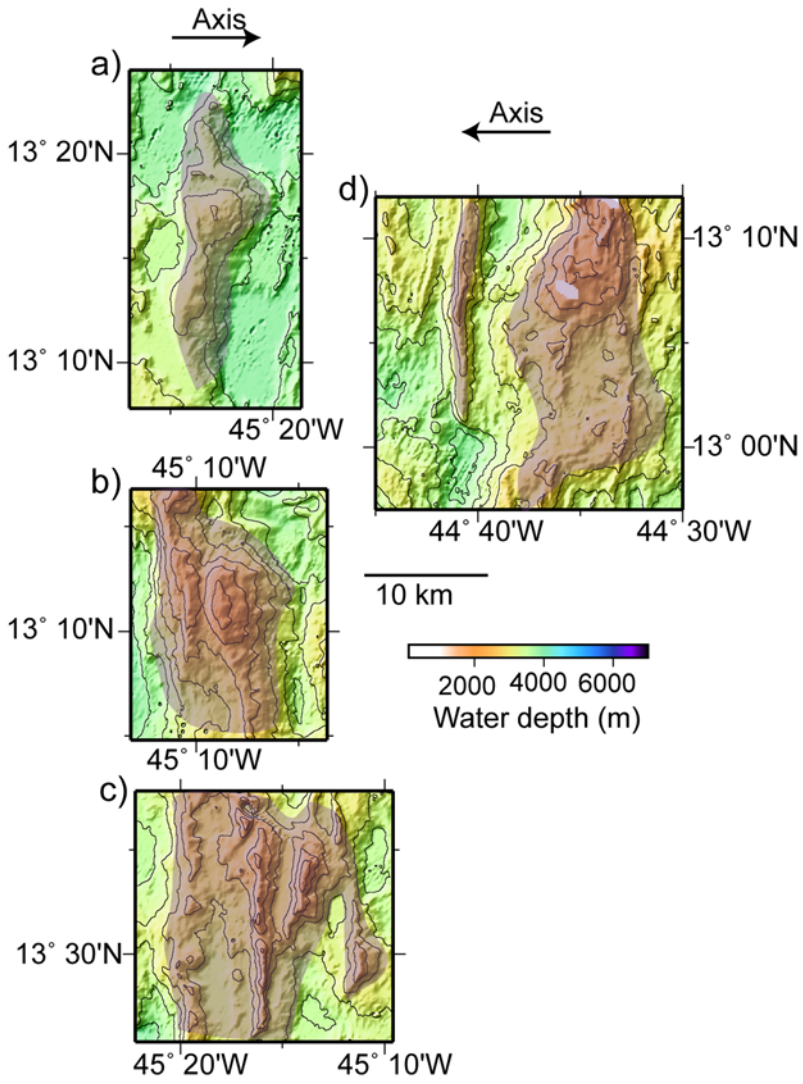

Figure 9. Examples of off-axis core complexes in the 13°N segment. Bathymetry maps are contoured at 250-m intervals and all are plotted at the same scale. Shading: interpretation of the core complex massif. (a), (b), and (c) Core complexes west of the spreading axis. (d) Core complex east of the spreading axis.

uniform magnetic source layer 1 km thick whose upper bound is the seafloor. Magnetization was assumed to be parallel to the field of a geocentric dipole. The data were bandpass filtered for wavelengths between 50 km and 3 km. No annihilator was added to the data. Crustal magnetization is shown in Figure 10 with anomaly picks. As a result of the wide 9-km track spacing the spatial resolution of the crustal magnetization south of 14°10′N is considerably lower than in the area to the north where data were collected at a 5-km track spacing [*Fujiwara et al.*, 2003]. We were aided in our interpretation of the magnetic data by the picks of *Fujiwara et al.* [2003]. The picks shown in Figure 10, however, are our own.

[32] In the 14°N segment, *Fujiwara et al.* [2003] identified well lineated, high amplitude, and symmetrical magnetic anomalies both near the axis and on its flanks, consistent with this segment being produced by typical symmetrical magmatic accretion at the spreading axis for the past several millions of years. In contrast, the anomalies for the 15°N segment are lower in amplitude and irregular to discontinuous. *Fujiwara et al.* [2003] noted the association of low amplitude, irregular magnetic patterns with elevated, irregular seafloor topography, and concluded that the 15°N segment has been dominated by amagmatic extension for the past 5 My.

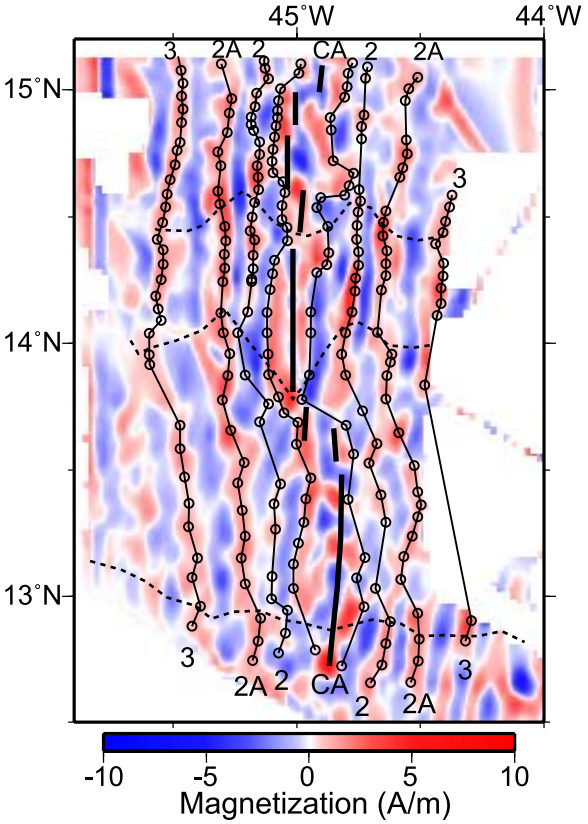

Figure 10. Crustal magnetization calculated for the region between the Fifteen-Twenty and Marathon fracture zones correcting for seafloor topography and removing skewness associated with the low latitudes of the study region. Data north of 14°10′N are from *Fujiwara et al.* [2003]. Circles: magnetic anomaly picks along the tracklines. Thick black line: spreading axis. Dashed lines: boundaries of the 14°N segment and in the south the boundary between detachment-fault-dominated terrain and volcanic terrain of the 13°N segment.

[33] Because of the lower spatial resolution south of 14°10′N only anomalies 3n, 2An, and 2n, the Brunhes-Matuyama boundary in the 14°N segment, and the boundary of un-identified high-amplitude axial anomalies in the 13°N and 15°N segments were identified (Figure 10). Anomalies in the southern half of the 14°N segment are well behaved, relatively high amplitude, and symmetrical about the spreading axis. In contrast, the anomalies in the 13°N segment are lower in amplitude and disrupted, similar to those in the 15°N segment. In particular, the Brunhes anomaly in the 13°N segment is so disrupted that it cannot be defined unambiguously at the present time. It is also difficult to relate the topographically defined spreading axis (interpreted as the locus of volcanism) to a Brunhes anomaly, which is not consistently symmetric about it. We identify anomalies more positively on the west flank of the 13°N segment (Figure 10). On the east flank, the data coverage is limited and anomaly identification more difficult.

6.2. Residual Topography

[34] We have used our magnetic anomaly picks to generate a grid of crustal ages and from this a subsidence grid based on the square root of crustal age subsidence curve and published parameters for the 13–15°N region [*Calcagno and Cazenave*, 1993]. Residual bathymetry was then calculated by subtracting the subsidence grid from the bathymetry grid. Figure 11 shows that the 14°N segment is significantly shallower than the 13°N and 15°N segments, which show local highs. Most of the identified core complexes are associated with these local highs, and thus core complex formation may be coeval with magmatism albeit at a reduced rate compared to normal magmatic accretion.

6.3. Mantle Bouguer and Residual Mantle Bouguer Gravity Anomalies

[35] The free-air gravity data (Figure 2c), which primarily reflect the gravity effect of seafloor topography, were reduced to obtain the mantle Bouguer and the residual mantle Bouguer anomalies (MBA and RMBA, respectively) following standard procedures [*Kuo and Forsyth*, 1988; *Prince and Forsyth*, 1988]. The effect of the water-crust and crust-mantle interfaces, assuming a crustal thickness of 5 km and a crustal density of 2750 kg/m^3, was calculated from the available bathymetry (Figure 2a) complemented with the satellite-derived global seafloor topography [*Smith and Sandwell*, 1997] elsewhere. This minimized the edge effects during upward continuation using Parker's method [*Parker*, 1973]. The predicted free air anomaly (FAA) was removed from the observed FAA along the ship tracks and gridded to obtain the MBA map (Figure 12a), which reflects both the mantle thermal structure and density variations in the shallow lithosphere. The gravity thermal effect due to spreading was calculated using a passive upwelling model, the ridge geometry [*Phipps Morgan and Forsyth*, 1988], and parameters used by *Escartín and Cannat* [1999]. The calculated thermal effect was then removed from the MBA along tracks to obtain the RMBA (Figure 12b), which can be interpreted in terms of density variations of the shallow lithosphere. To first order,

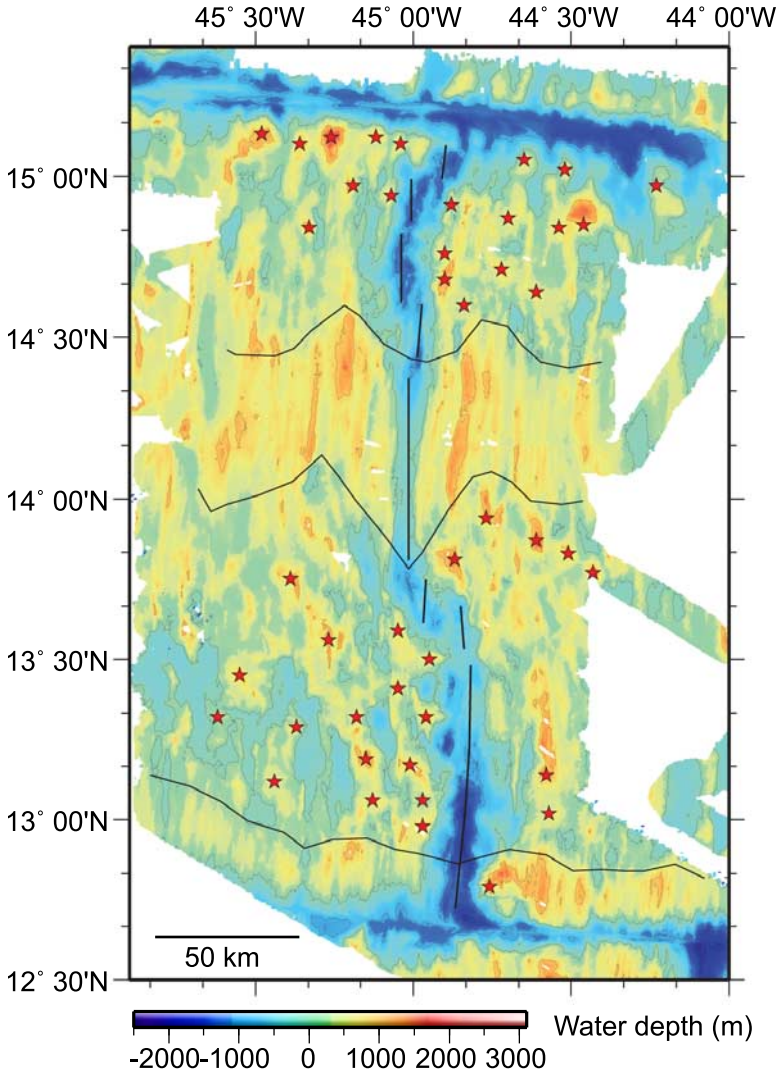

Figure 11. Residual bathymetry calculated by subtracting the predicted seafloor subsidence with age from the bathymetry grid. Red stars: locations of the core complexes identified in Figure 7b.

the RMBA is a proxy for crustal thickness [e.g., *Kuo and Forsyth*, 1988]. We inverted the RMBA [*Parker and Huestis*, 1974] to predict the variations in thickness assuming a crustal density of 2750 kg/m^3, as shown in Figure 12c. Calculated crustal thickness, particularly in the core complex terrain, is thus the maximum estimate of the overall magmatic crustal thickness and therefore magmatic production. At least a portion of this 'crustal thickness' corresponds to altered mantle rocks, instead of magmatic rocks, as the outcrop of altered peridotites in this area demonstrates [e.g., *Cannat et al.*, 1997; *Lagabrielle et al.*, 1998].

[36] As described above, lineated volcanic terrain dominates the crust formed along the 14°N segment and at the southern end of the 13°N segment immediately north of the Marathon fracture zone. The seafloor in the remaining sections of the 13°N segment, and the 15°N is characterized by fault rotation and core complexes. The core complex terrain is systematically associated with elevated RMBA values (~25–50 mgals higher than those in the 14°N segment, Figure 12b), which may be interpreted as a reduction in crustal thickness of at least 1 km with respect to the lineated terrain (Figure 12c). This correlation between core complex terrain and associated thin crust has been observed near the Fifteen-Twenty fracture zone [*Escartín and Cannat*, 1999; *Fujiwara et al.*, 2003], where it was ascribed to cooling near a large-offset fracture zone [e.g., *Escartín and Cannat*, 1999]. In our study area, however, not only does the high RMBA and inferred crustal thinning extend far from any fracture zone, but in

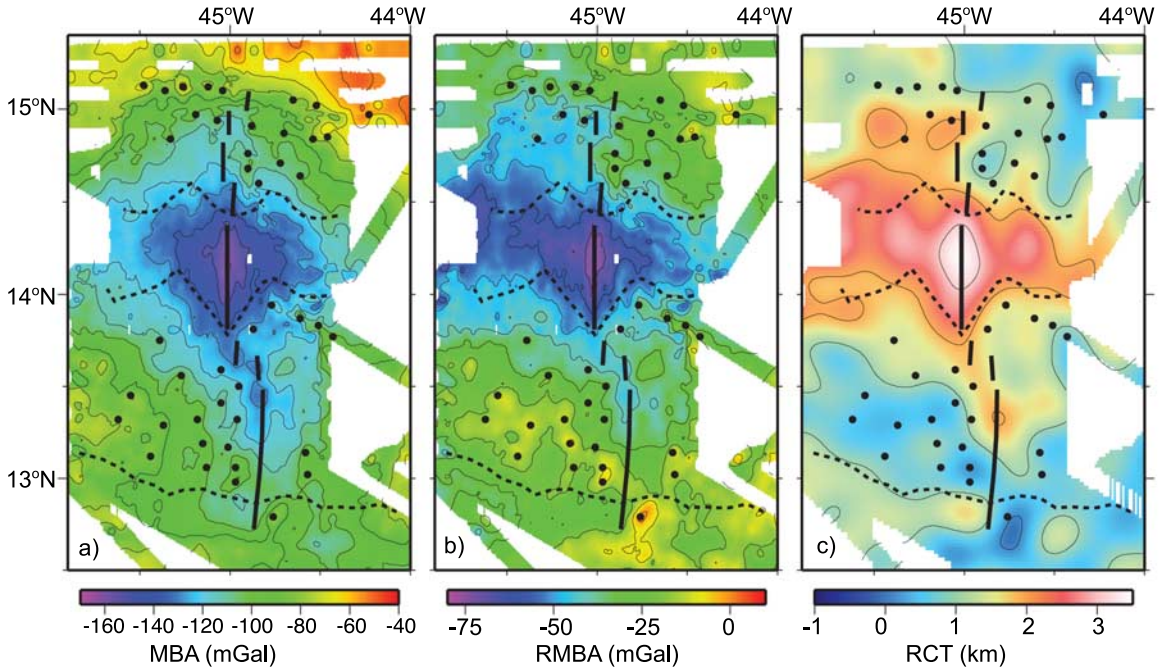

Figure 12. (a) Mantle Bouguer anomaly (MBA), which reflects both the mantle thermal structure and density variations in the shallow lithosphere. (b) Residual mantle Bouguer anomaly (RMBA) calculated by removing the thermal effect from the MBA. RMBA can be interpreted in terms of density variations of the shallow lithosphere. To first order, the RMBA is a proxy for crustal thickness and therefore, of overall magmatic supply. (c) Residual crustal thickness (RCT) calculated from the RMBA. Black dots: core complexes identified in Figure 7b. Black line: spreading axis. Dashed lines: boundaries of the 14°N segment and in the south, the boundary between detachment-fault-dominated terrain and volcanic terrain of the 13°N segment.

the 13°N segment lineated volcanic morphology has formed close to the Marathon fracture zone associated with high RMBA values.

7. Discussion

[37] Between the Fifteen-Twenty and Marathon fracture zones there are a variety of seafloor morphologies that we now recognize as significantly rotated faults and core complexes. In the following we review the diagnostic features of the core complexes we have identified and attempt to answer some of the questions they raise.

7.1. Fault Rotation and Detachment Faulting

[38] We infer above that the 20–30° outward-facing slopes in the 13°N and 15°N segments (Figure 6) result from outward rotation of the originally subhorizontal median valley floor while the inward-facing slopes represent rotated normal faults. Fault rotation by as much as 20° occurs within 5 km of the volcanic axis, or <2 km from the point of initiation of the fault (Figures 3, 4, 6, and 13a). Because the across-axis distance over which the initial rotation occurs is small, the fault must be steep at depth and roll over quickly with distance to the axis.

[39] Significant footwall rotation has been inferred from paleomagnetic data from drill sites in the region. The Logachev massif and a topographic high on the conjugate side of the axis show rotations of 50°–80° at ~1 My [*Garces and Gee*, 2007]. Just north of the Fifteen-Twenty fracture zone, the footwall of the detachment at 15°45′N shows rotations of ~40° [*Carlut et al.*, 2006]. Significant rotation of a section of ocean crust has also been documented from a drill hole off-axis in the western North Atlantic [*Schouten*, 2002]. *Buck* [1988] has modeled this large and rapid flexural rotation of steep normal faults with an elastic thickness Te < 1 km; models with a larger Te produce the same magnitude rotation but at proportionally greater extension.

[40] If extension on a single fault continues for more than about 5 km, the exhumed fault surface flattens and domes as a result of regional isostatic compensation [e.g., *Buck*, 1988] (Figure 13b). The

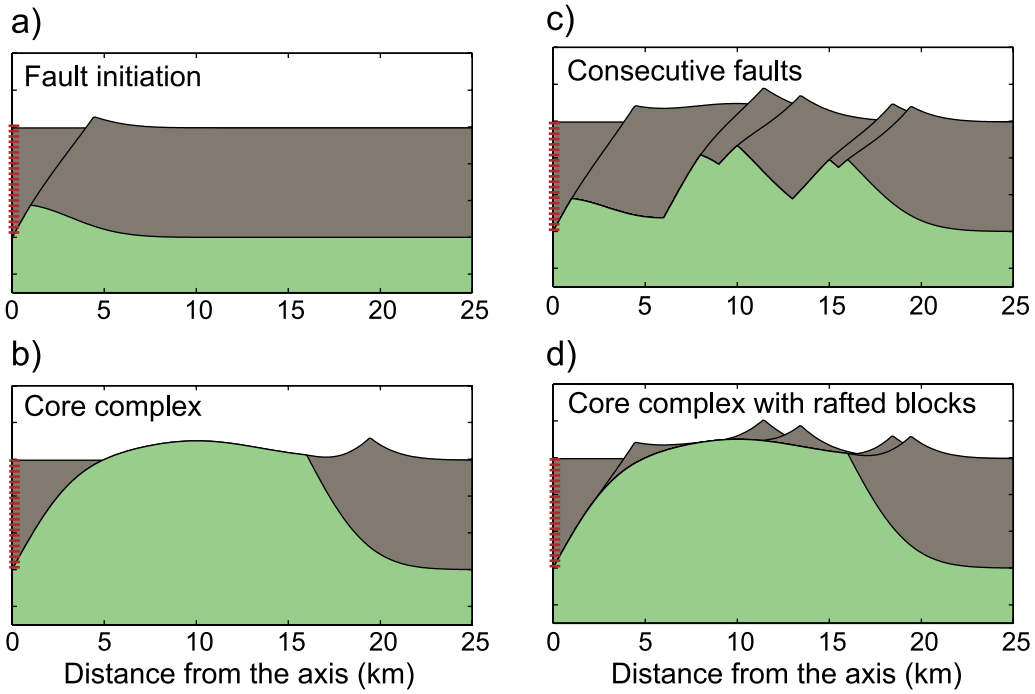

Figure 13. Four cartoons for the evolution of detachment faulting. (a) A normal fault at the axis. Flexural rotation of the fault results in the formation of a linear ridge and backing basin. Fault offset = 1 km; fault rotation = 18°. (b) Continued extension on the detachment fault increases the rotation of the fault and exposes lower crustal rocks and a corrugated footwall. Fault offset = 16 km; fault rotation = 36°. (c) Consecutive faults. In this case most of the lithosphere is accreted through typical magmatic processes at slow-spreading ridges. (d) Continuous detachment fault. New faults formed at the axis root into the main detachment. Triangular sections of median valley floor are transferred from the hanging wall to the footwall of the fault and rafted off axis. Gaps between rafted blocks may expose the primary detachment surface, which may show corrugations. The cartoons simulate regional isostatic compensation and use the flexural rotation of 60° normal faults for an effective elastic thickness of lithosphere Te = 0.4 km [e.g., *Buck*, 1988]. Gray on the figure is crust predating the onset of faulting and green is material from below drawn up during the slip on the fault and its rotation.

exhumed fault may be exposed at the seafloor and show corrugations running parallel to the spreading direction. Within our survey area, individual corrugations on the footwall may run for more than 10 km and the rather irregular pattern of corrugations on the fault plane remains unchanged during that amount of slip. The corrugations emerge already formed from beneath the hanging wall and show no sign of changing shape as the slip on the fault continues. The simplest explanation for these observations is that the corrugated pattern is impressed by a brittle hanging wall on a more ductile footwall, in the mechanism of continuous casting suggested by *Spencer* [1999]. This mechanism is the same as that used to create extruded metal or plastic, where a cooled die impresses the required pattern on the ductile extruding metal or plastic.

[41] In the 13°N segment the morphology of individual near-axis core complexes (Figure 3b) suggests that they accommodate between 8 and 12 km of extension, corresponding to lifetimes of 0.7–1.0 My assuming symmetrical spreading. There are several places, however, where prominent linear ridges, indicating significant rotation, are spaced much more closely together with no corrugations showing between them. The simplest interpretation of this morphology is that it represents a succession of rotated normal faults, each fault accommodating less than a few km of extension before the next one forms (Figure 13c). Another interpretation is that the normal faults are rooted into the same detachment [*Buck*, 1988] (Figure 13d). In this case, the ridges are triangular sections of the median valley floor hanging wall, which we refer to as rafted blocks, and corrugations may be found between them.

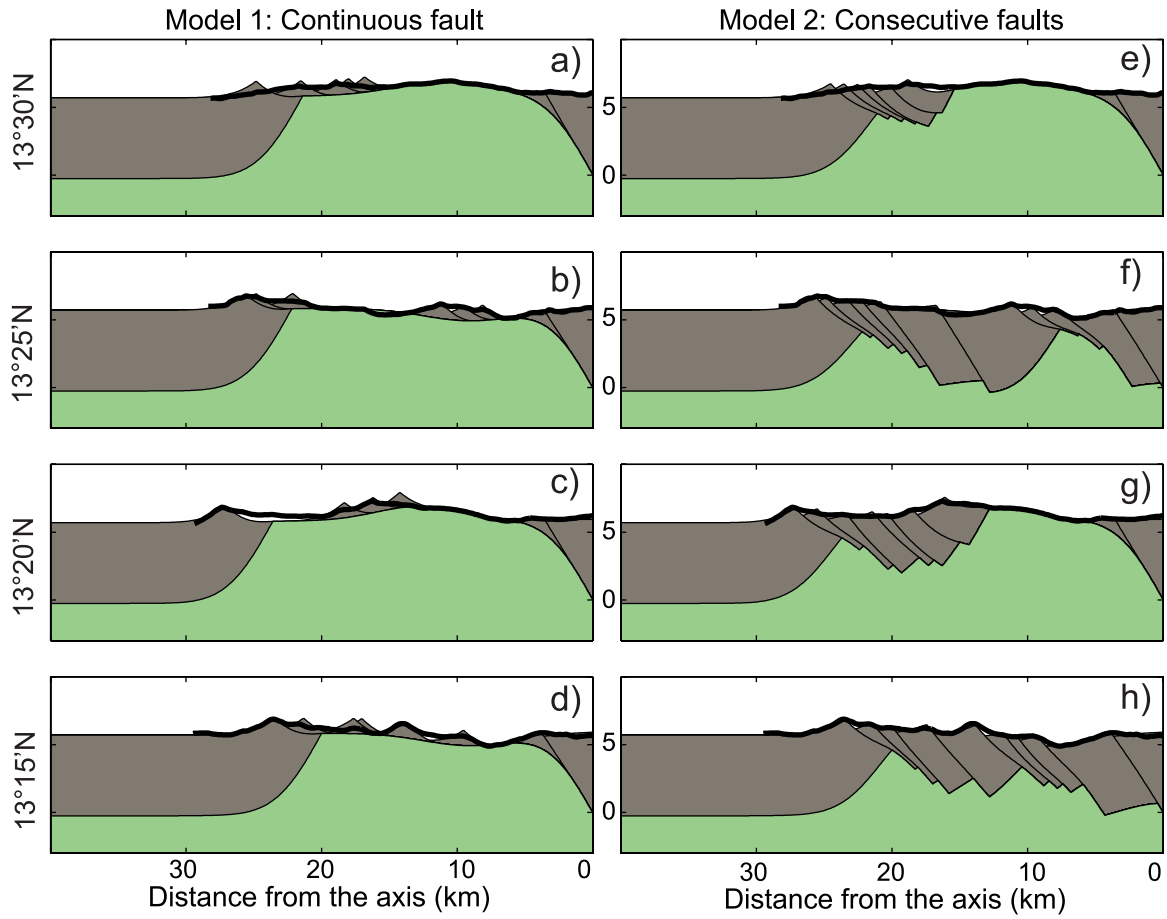

Figure 14. Two models for detachment fault formation and evolution in the region of the 13°N segment shown in Figure 3. Thick black lines: seafloor topography at no vertical exaggeration from the profiles in Figure 3c. (left) A single long-lived detachment fault that is continuous along the axis. New normal faults at the axis root into the main detachment. Sections of median valley floor are transferred from the hanging wall to the footwall. Most of the oceanic lithosphere is accreted through uplift of mafic and ultramafic rocks. (right) Successive detachment faults, which are discontinuous along the axis. Occasionally new faults at the axis root into a detachment surface to transfer a section of median valley floor hanging wall to the footwall. A large part of the oceanic lithosphere is formed by typical magmatic processes at slow-spreading ridges. The models simulate regional isostatic compensation and use the flexural rotation of 60° normal faults for an effective elastic thickness of lithosphere Te = 0.4 km [e.g., *Buck*, 1988]. Gray: crust predating the onset of faulting. Green: material from below drawn up during the slip on the fault and its rotation.

[42] From multibeam bathymetry (gridded at 150 m) it is impossible to distinguish between the interpretations demonstrated in Figures 13c and 13d. Consequently, we present both interpretations (Figure 14) of the multiple core complex morphology near the axis in the 13°N segment (lines shown in Figure 3b). In the continuous fault interpretation of Figures 14a–14d we assume that the linear ridges on the domes at 13°30′N and 13°20′N, and in the intervening swales at 13°25N and 13°15N, are rotated faults that root into one continuous detachment surface along this length of the 13°N segment. We assume that detachment faulting initiated almost simultaneously along the major chain of linear ridges running north to south along 45°04′W about 25 km west of the axis (see Figure 3b). This means that the linear ridges east of 45°04′W are triangular slivers of median valley floor hanging wall resting atop the detachment like those depicted in Figure 13d; corrugations may be observed on the detachment surface exposed between them.

[43] In the consecutive fault interpretation of Figures 14e–14h no single detachment is assumed and most of the linear ridges are separate rotated

normal faults with less than a few km extension. We model large offset single detachments only where corrugations can be observed on the domes crossed at 13°20′N and 13°30′N, all other linear ridges were modeled using a succession of normal faults.

[44] Clearly the interpretation of detachment fault initiation and extent across the axis from bathymetry data is ambiguous. Because of this we have avoided using the term "breakaway" in this paper, which is commonly taken to mean the site where the detachment fault first breaks out at the seafloor.

[45] When we consider the along-axis extent of a single detachment fault in Figures 14a–14d, the bathymetric morphology of the 13°N segment suggests that at present active detachment faulting may be occurring on a single fault plane that extends most of the length of the spreading segment on its western side. At the seafloor the present-day faulting is divided into a number of individual sections which have been described above. Some of these sections are dome-shaped corrugated highs (massifs '1' and '2' on Figure 3a), while others are basins between the highs. These different segments are joined end to end along axis, in some places more or less directly, and in others with a small offset. At those offsets there must be some sort of accommodation between the two segments, perhaps a minor strike-slip relay zone, but these cannot be seen from the bathymetry.

[46] If all of the different sections root in a single major detachment at depth (as in Model 1 of Figure 14) and only split as they rise to the surface, then there must be considerable along-axis relief on the underlying detachment plane perhaps constrained by variable uplift on the hanging wall. The horizontal distance between the summits of core complex domes and the bottom of adjacent basins is about 10 km, while the difference in seafloor depth between the tops of the core complexes and the bottoms of the basins may reach 2000 m. This is an order of magnitude greater relief than that of the corrugations on the detachment fault surfaces exposed on the seafloor.

[47] We have suggested the possibility of nearly simultaneous initiation of new detachment faults along the length of the segment at a chain of outward-facing slopes along 45°04′W, ~25 km off-axis. A second row of core complexes is found ~15 km farther west, which could well have been active all at the same time too (along ~45°12′W on Figure 7a). Additional data will be needed to constrain more fully the along and across axis extent of a single detachment fault and the nature of its bounds.

7.2. Implications for the Accretion of Oceanic Lithosphere

[48] The two models we have proposed for core complex formation have profoundly different implications for the mode of accretion of oceanic lithosphere, and for the transfer of hanging wall material to the footwall by detachment-related faulting near the axis. Model 1, a single long-lived detachment fault, requires that most of the lithosphere is formed by detachment spreading and uplift of mafic and ultramafic rocks. Model 2, a series of faults two of which have significant extension and have formed the core complexes at 13°30′N and 13°20′N, requires that lithospheric accretion driven by extension along detachments is a minor component compared to that accreted by typical magmatic spreading at slow-spreading segments. Model 2 also requires relay zones along axis accommodating the links between individual faults.

[49] Ambiguity in our being able to choose between these models arises because the interpretation of the bathymetric morphology is subjective and not a reliable indicator of the lithology exposed at the seafloor. For example, we can not be sure whether the deep basins form as a flexural response to fault rotation or are exposed sections of the detachment. Near to the axis the basins can be deeper than the axial valley floor, which is difficult to explain. Based on the high rate of hydroacoustically-recorded seismic activity observed in this area [*Escartín et al.*, 2003b; *Smith et al.*, 2003], and the delineation by microearthquakes of the fault zone associated with the core complex at the TAG segment at 26°N [*deMartin et al.*, 2007], a microseismicity study of this region would help to constrain the geometry of the faults at depth.

7.3. Magmatism and Detachment Faulting

[50] Numerical models of the role of faulting in the generation of new lithosphere [*Buck*, 1988; *Buck et al.*, 2005] show that detachment faults form when magma supply is decreased. When magmatic spreading is reduced to 50% of total spreading and restricted to one side of the axis, a single fault forms on the opposite side and accommodates long-lived slip, while its footwall rolls over to form characteristic topography that we associate with

oceanic core complexes (e.g., frequently an elevated linear ridge where the fault initiates and an elevated dome).

[51] Both the gravity data (Figure 12) and the residual bathymetry (Figure 11) from our study area support the conclusions from the numerical models of reduced magma supply triggering the formation of detachments [*Buck*, 1988; *Buck et al.*, 2005]. In the regions containing abundant core complexes and other evidence of detachment faulting (13°N and 15°N segments), the data indicate relatively thinner crust in comparison to the volcanically-dominated seafloor in the 14°N segment which produces long, linear volcanic abyssal hills with steep inward-facing slopes on both flanks.

[52] The frequent sampling and drilling of gabbro bodies in the upper parts of core complexes [*Blackman et al.*, 2002; *Dick et al.*, 2000; *Escartín et al.*, 2003a; *Ildefonse et al.*, 2007; *MacLeod et al.*, 2002; *Tucholke et al.*, 1998, 2005] suggests, however, that the magmatic contribution to the lithosphere in these regions is not restricted to the conjugate side of the axis as assumed by the numerical models; but that instead, there is a magmatic component to spreading on both sides of the axis during core complex formation. The proportion of magma to each flank is not well constrained by the existing data at this time.

[53] Because of the overall reduced magma supply to the ridge it is likely that core complex formation is associated with diagnostic topography on the opposite flank. To test this idea, it will be important to examine more closely the morphology generated on the opposite flank during detachment faulting. We observe in some places that the conjugate flank has a relative deep that is similar in size to the massif developed during core complex formation (e.g., massif at 13°47′N, 44°45′W and deep at 14°05′N, 45°20′W). This might support the idea that less melt was available for magmatic spreading for the period that the detachment was slipping, but additional studies are needed to confirm this.

7.4. Equatorial Atlantic

[54] On a regional scale, our interpretation of the bathymetry of our study area indicates that two thirds of the plate boundary between the Fifteen-Twenty and Marathon fracture zones is extending principally by detachment faulting. Why are detachment faulting and core complex formation so prevalent in this region? Data from rock sampling in the vicinity of the 14°N segment [*Bougault et al.*, 1988; *Dosso et al.*, 1993; *Staudacher et al.*, 1989] show a localized geochemical enrichment centered at 14°N and displays elevated incompatible trace element (e.g. La/Sm, K/Ti and Nb/Zr) and isotope ratios (e.g., 87Sr/86Sr > 0.7028; 206Pb/204Pb > 19.0). The origin of this geochemical anomaly and particularly its localized nature has attracted a good deal of interest and speculation [e.g., *Bougault et al.*, 1988]. *Bougault et al.* [1988] have suggested that the development of some triple junctions is associated with a rising mantle plume. Compared to other plumes, however, the 14°N anomaly is subdued, suggesting that both the plume and triple junction in this area may be embryonic, or correspond to a localized mantle heterogeneity.

[55] Is the apparent magma deficit and the associated anomalous composition of the magmas erupted associated in some way with the proximity of this area to the NA-SA-AF triple junction? Though the relative velocity between NA and SA in this region is very small, the resultant deformation may be responsible not only for the off-axis seismicity (Figure 1) [*Escartín et al.*, 2003b] but also for the anomalous behavior of the mantle. We suspect that in other regions of the oceans where magma supply is limited or varies dramatically along the axis, core complex formation may also be widespread.

8. Conclusions

[56] The topography of the 15°N and 13°N segments between the Fifteen-Twenty and Marathon fracture zones is dominated by flexural rotation of normal faults (outwardly rotated seafloor generating linear ridges) and core complex formation (low-angle normal fault surfaces). We have identified 45 potential core complexes within these two segments (Figure 7). The abundance of examples of core complexes with different morphologies (Figures 8 and 9) and with different spatial relationships has allowed us to reach some clear-cut conclusions on their formation and evolution.

[57] Our measurements of outward-facing slopes of linear ridges indicate that normal faults undergo rotations of as much as 20° within a few kilometers of the volcanic axis (Figure 6). An additional 10°–15° of rotation may occur before rotation is complete at 10–15 km from the axis (~1 My). We suggest that the unusually large rotation of faults in the 13° and 15°N segments indicates that these segments are undergoing large amounts of tectonic

extension on single faults. The extent and rapidity of the rotation indicates that the associated faults steepen very rapidly with depth close to the volcanic axis. Fault rotation can be modeled with the flexural rotation of a 60° normal fault assuming effective elastic thickness of the lithosphere, Te < 1 km [e.g., *Buck*, 1988] (Figure 6).

[58] Linear ridges are frequently linked to low-angle, corrugated detachment surfaces that are interpreted to cap core complex domes showing that the exhumed detachment surfaces roll over to nearly horizontal as they evolve and spread away.

[59] Two models for core complex formation fit our observations of multiple core complexes separated by swales in the 13°N segment (Figure 14). In Model 1 a single detachment fault is long-lived and continuous along the axis and requires that most of the lithosphere is formed by passive uplift of mafic and ultramafic rocks. In Model 2 faults form in succession with more limited extension, and are discontinuous along the axis. Faulting alternates with magmatic spreading typical at slow-spreading segments. We are not able to choose between these two models of detachment formation for the features in our study area with the existing data.

[60] The mantle in our study region may be unusual and associated with the nearby NA-SA-AF triple junction. Gravity data show that melt production is limited in the region, except at the 14°N segment (Figure 12), creating the conditions that encourage the formation of detachment faulting. We suspect that in other regions of the oceans where magma supply is limited or varies dramatically along the axis such as in our study area, core complex formation may be widespread as well.

Acknowledgments

[61] We would like to thank P. Lemmond and the captain and crew of the R/V *Knorr* for their help in collecting the data used in this study. M. Tivey was instrumental in diagnosing a problem with the magnetometer during the cruise. We would also like to thank T. Fujiwara for providing us with the data for the region of the Fifteen-Twenty fracture. M. Cannat kept us up-to-date on the findings of the "Serpentine" cruise of the R/V *Porquoi Pas*? in Spring 2007. We thank R. Garcia (U. Girona, Spain) for producing photomosaics. We had helpful discussions with B. Tucholke, M. Tivey, R. Reeves-Sohn, and J. Spencer. This paper benefited from the reviews of B. John and L. Lavier. D. Smith and H. Schouten were supported in this work by NSF grant OCE-0649566. J. Escartín was supported by CNRS. This is IPGP contribution 2297.

References

Beltnenev, V., et al. (2003), New discoveries at the 12°58′N, 44°52′N, MAR: Professor Logachev-22 cruise, initial results, *InterRidge News*, *12*, 13–14.

Blackman, D. K., J. R. Cann, B. Janssen, and D. K. Smith (1998), Origin of extensional core complexes: Evidence from the Mid-Atlantic Ridge at Atlantis Fracture Zone, *J. Geophys. Res.*, *103*, 21,315–21,333.

Blackman, D. K., et al. (2002), Geology of the Atlantis Massif (Mid-Atlantic Ridge, 30°N): Implications for the evolution of an ultramafic oceanic core complex, *Mar. Geophys. Res.*, *23*, 443–469.

Bogdanov, Y., A. Sagalevitch, E. Chernyaev, A. Ashadze, E. Gurvich, V. Lukashin, G. Ivanov, and G. Peresypkin (1995), A study of the hydrothermal field at 14°45′N on the Mid-Atlantic Ridge using the MIR submersibles, *BridgeNews*, *9*, 9–14.

Bohnenstiehl, D. R., M. Tolstoy, R. P. Dziak, C. G. Fox, and D. K. Smith (2002), Aftershock sequences in the mid-ocean ridge environment: An analysis using hydroacoustic data, *Tectonophysics*, *354*, 49–70.

Bonatti, E. (1996), Long-lived oceanic transform boundaries formed above mantle thermal minima, *Geology*, *24*(9), 803–806.

Bougault, H., L. Dimitriev, J. G. Schilling, A. Sobolev, J. L. Joron, and H. D. Needham (1988), Mantle heterogeneity from trace elements: MAR triple junction near 14°N, *Earth Planet. Sci. Lett.*, *88*, 27–36.

Buck, R. W. (1988), Flexural rotation of normal faults, *Tectonics*, *7*(5), 959–973.

Buck, W. R., L. L. Lavier, and A. N. B. Poliakov (2005), Modes of faulting at mid-ocean ridges, *Nature*, *434*, 719–723.

Calcagno, P., and A. Cazenave (1993), Present and past regional ridge segmentation: evident in geoid data, *Geophys. Res. Lett.*, *20*(18), 1895–1898.

Canales, J. P., R. A. Sohn, and B. J. deMartin (2007), Crustal structure of the TAG segment (Mid-Atlantic Ridge, 26°10′N): Implications for the nature of hydrothermal circulation and detachment faulting at slow spreading ridges, *Geochem. Geophys. Geosyst.*, *8*, Q08004, doi:10.1029/2007GC001629.

Cann, J. R., D. K. Blackman, D. K. Smith, E. McAllister, B. Janssen, S. Mello, E. Avgerinos, A. R. Pascoe, and J. Escartín (1997), Corrugated slip surfaces formed at North Atlantic ridge-transform intersections, *Nature*, *385*, 329–332.

Cannat, M., and J. F. Casey (1995), An ultramafic lift at the Mid-Atlantic Ridge: Successive stages of magmatism in serpentinized peridotites from the 15°N region, in *Mantle and Lower Crust Exposed in Oceanic Ridges and in Ophiolites*, edited by R. L. M. Vissers and A. Nicolas, pp. 5–34, Kluwer Acad., Dordecht, Netherlands.

Cannat, M., D. Bideau, and H. Bougault (1992), Serpentinized peridotites and gabbros in the Mid-Atlantic Ridge axial valley at 15°37′N and 16°52′N, *Earth Planet. Sci. Lett.*, *109*, 87–106.

Cannat, M., et al. (1995), Thin crust, ultramafic exposures, and rugged faulting patterns at the Mid-Atlantic Ridge (22°–24°N), *Geology*, *23*, 49–52.

Cannat, M., Y. Lagebrielle, H. Bougault, J. Casey, N. D. Coutures, L. Dmitriev, and Y. Fouquet (1997), Ultramafic and gabbroic exposures at the Mid-Atlantic Ridge: Geological mapping in the 15°N region, *Tectonophys.*, *279*, 193–213.

Cannat, M., D. Sauter, V. Mendel, E. Ruellan, K. Okino, J. Escartin, V. Combier, and M. Baala (2006), Modes of seafloor generation at a melt-poor ultraslow-spreading ridge, *Geology*, *34*(7), 605–608.

Carlut, J., C. MacLeod, H. Horen, and J. Escartín (2006), Paleomagnetic results from a mid-ocean ridge detachment at the Mid-Atlantic Ridge, 15°45′N, paper presented at EGU Meeting, Vienna.

Christie, D. M., B. P. West, D. G. Pyle, and B. B. Hanan (1998), Chaotic topography, mantle flow and mantle migration in the Australian-Antarctic discordance, *Nature*, *394*(6694), 637–644.

Collette, B. J., K. Rutten, H. Schouten, and A. P. Slootweg (1974), Continuous seismic and magnetic profiles over the Mid-Atlantic Ridge between 12° and 18°N, *Mar. Geophys. Res.*, *2*, 133–141.

deMartin, B. J., R. A. Reves-Sohn, J. P. Canales, and S. E. Humphris (2007), Kinematics and geometry of active detachment faulting beneath the TAG hydrothermal field on the Mid-Atlantic Ridge, *Geology*, *35*(8), 711–714.

DeMets, C., R. G. Gordon, D. F. Argus, and S. Stein (1994), Effect of recent revisions to the geomagnetic reversal time scale on estimates of current plate motions, *Geophys. Res. Lett.*, *21*(20), 2191–2194.

Dick, H. J. B., G. Thompson, and W. B. Bryan (1981), Low angle faulting and steady-state emplacement of plutonic rocks at ridge-transform intersections (abstract), *Eos Trans. AGU*, *62*, 406.

Dick, H. J. B., et al. (2000), A long in situ section of the lower ocean crust: Results of ODP leg 176 drilling at the Southwest Indian Ridge, *Earth Planet. Sci. Lett.*, *179*(31–51), doi:10.1016/S0012-1821X(1000)00102-00103.

Dixon, T. H., and A. Mao (1997), A GPS estimate of relative motion between North and South America, *Geophys. Res. Lett.*, *24*, 535–538.

Dosso, L., H. Bougault, J. G. Schilling, and J.-L. Joron (1991), Sr-Nd-Pb geochemical morphology between 10° and 17°N on the Mid-Atlantic Ridge: a new MORB isotope signature, *Earth Planet. Sci. Lett.*, *106*, 29–43.

Dosso, L., H. Bougault, and J.-L. Joron (1993), Geochemical morphology of the North Mid-Atlantic Ridge, 10°–24°N: trace element-isotope complementarity, *Earth Planet. Sci. Lett.*, *120*, 443–462.

Dziak, R., D. Smith, D. Bohnenstiehl, C. Fox, D. Desbruyeres, H. Matsumoto, M. Tolstoy, and D. Fornari (2004), Evidence of a recent magma dike intrusion at the slow-spreading Lucky Strike segment, Mid-Atlantic Ridge, *J. Geophys. Res.*, *109*, B12102, doi:10.1029/2004JB003141.

Escartín, J., and M. Cannat (1999), Ultramafic exposures and the gravity signature of the lithosphere near the Fifteen-Twenty Fracture Zone (Mid-Atlantic Ridge, 14° – 16.5°N), *Earth Planet. Sci. Lett.*, *171*, 411–424.

Escartín, J., C. Mével, C. J. MacLeod, and A. M. McCaig (2003a), Constraints on deformation conditions and the origin of oceanic detachments: The Mid-Atlantic Ridge core complex at 15°45′N, *Geochem. Geophys. Geosyst.*, *4*(8), 1067, doi:10.1029/2002GC000472.

Escartín, J., D. K. Smith, and M. Cannat (2003b), Parallel bands of seismicity at the Mid-Atlantic Ridge, 12–14N, *Geophys. Res. Lett.*, *30*(12), 1620, doi:10.1029/2003GL017226.

Fujiwara, T., J. Lin, T. Matsumoto, P. B. Kelemen, B. E. Tucholke, and J. F. Casey (2003), Crustal evolution of the Mid-Atlantic Ridge near the Fifteen-Twenty Fracture Zone in the last 5 Ma, *Geochem. Geophys. Geosyst.*, *4*(3), 1024, doi:10.1029/2002GC000364.

Garces, M., and J. S. Gee (2007), Paleomagnetic evidence of large footwal rotations associated with low-angle faults at the Mid-Atlantic Ridge, *Geology*, *35*, 279–282.

IAGA, (1996), International Association of Geomagnetism and Aeronomy, Division V, Working Group 8, International geomagnetic reference field, 1995 revision, *Geophys. J. Int.*, *125*, 318–321.

Ildefonse, B., D. K. Blackman, B. E. John, Y. Ohara, D. J. Miller, and C. J. MacLeod (2007), Oceanic core complexes and crustal accretion at slow-spreading ridges, *Geology*, *35*, 623–626.

Javoy, M., and F. Pineau (1991), The volatiles record of a "popping" rock from the Mid-Atlantic Ridge at 14°N: chemical and isotopic composition of gas trapped in the vesicles, *Earth Planet. Sci. Lett.*, *107*, 598–611.

Jones, E. J. W. (1987), Fracture zones in the equatorial Atlantic and the breakup of western Pangea, *Geology*, *15*, 533–536.

Kelemen, P. B., et al. (2004), Proc. ODP, in *Init. Repts.*, doi:10.2973/odp.proc.ir.2209.2004, Ocean Drilling Program, College Station, Tex.

Klitgord, K. D., and H. Schouten (1986), Plate kinematics of the central Atlantic, in *The Geology of North America*, vol. M, *The Western North Atlantic Region*, edited by P. R. Vogt and B. E. Tucholke, pp. 351–378, Geol. Soc. of Am., Boulder, Colo.

Kuo, B. Y., and D. W. Forsyth (1988), Gravity anomalies of the ridge-transform system in the South Atlantic between 31° and 34.5°S: Upwelling centers and variations in crustal thickness, *Mar. Geophys. Res.*, *10*, 205–232.

Lagabrielle, Y., D. Bideau, M. Cannat, J. A. Karson, and C. Mével (1998), Ultramafic-mafic plutonic rock suites exposed along the Mid-Atlantic Ridge (10°N–30°N): Symmetrical-asymmetrical distribution and implications for seafloor spreading processes, in *Faulting and Magmatism at Mid-Ocean Ridges*, edited by W. R. Buck, pp. 153–176, AGU, Washington, D. C.

LePichon, X., and P. J. Fox (1971), Marginal offsets, fracture zones, and the early opening of the North Atlantic, *J. Geophys. Res.*, *76*, 6294–6308.

MacLeod, C. J., et al. (2002), Direct geological evidence for oceanic detachment fauling: The Mid-Atlantic Ridge, 15°45′N, *Geology*, *30*(10), 279–282.

Müller, R. D., and W. H. F. Smith (1993), Deformation of the oceanic crust between the North American and South American plates, *J. Geophys. Res.*, *98*, 8275–8291.

Ohara, Y., T. Yoshida, and S. Kasuga (2001), Giant megamullion in the Perece Vela Backarc basin, *Mar. Geophys. Res.*, *22*, 47–61.

Parker, R. L. (1973), The rapid calculation of potential anomalies, *Geophys. J. R. Astron. Soc.*, *31*, 447–455.

Parker, R. L., and S. P. Huestis (1974), The inversion of magnetic anomalies in the presence of topography, *J. Geophys. Res.*, *79*, 1587–1593.

Phipps Morgan, J., and D. W. Forsyth (1988), Three-dimensional flow and temperature perturbations due to a transform offset: Effects on oceanic crustal and upper mantle structure, *J. Geophys. Res.*, *93*, 2955–2966.

Prince, R. A., and D. W. Forsyth (1988), Horizontal extent of anomalously thin crust near the Vema Fracture Zone from the three-dimensional analysis of gravity anomalies, *J. Geophys. Res.*, *93*, 8051–8063.

Sarda, P., and D. Graham (1990), Mid-ocean ridge popping rocks: implications for degassing at ridge crests, *Earth Planet. Sci. Lett.*, *97*, 268–289.

Schouten, H. (2002), Paleomagnetic inclinations in DSDP Hole 417D reconsidered: Secular variation or variable

tilting?, *Geophys. Res. Lett.*, *29*(7), 1103, doi:10.1029/2001GL013581.

Schroeder, T., M. Cheadle, H. J. B. Dick, U. Faul, J. F. Casey, and P. B. Kelemen (2007), Non-volcanic seafloor spreading and corner-flow rotation accommodated by extensional faulting at 15°N on the Mid Atlantic Ridge: A structural synthesis of ODP Leg 209, *Geochem. Geophys. Geosyst.*, *8*, Q06015, doi:10.1029/2006GC001567.

Searle, R. C., M. Cannat, K. Fujioka, C. Mevel, H. Fujimoto, A. Bralee, and L. Parson (2003), FUJI Dome: A large detachment fault near 64 degrees E on the very slow-spreading Southwest Indian Ridge, *Geochem. Geophys. Geosyst.*, *4*(8), 9105, doi:10.1029/2003GC000519.

Sella, G. F., T. H. Dixon, and A. Mao (2002), REVEL: A model for recent plate velocities from space geodesy, *J. Geophys. Res.*, *107*(B4), 2081, doi:10.1029/2000JB000033.

Sempéré, J.-C., J. Lin, H. S. Brown, H. Schouten, and G. M. Purdy (1993), Segmentation and morphotectonic variations along a slow-spreading center: The Mid-Atlantic Ridge (24°00′N–30°40′N), *Mar. Geophys. Res.*, *15*, 153–200.

Smith, D. K., M. Tolstoy, C. G. Fox, D. R. Bohnenstiehl, H. Matsumotu, and M. J. Fowler (2002), Hydroacoustic monitoring of seismicity at the slow-spreading Mid-Atlantic Ridge, *Geophys. Res. Lett.*, *29*(11), 1518, doi:10.1029/2001GL013912.

Smith, D. K., J. Escartin, M. Cannat, M. Tolstoy, C. G. Fox, D. Bohnenstiehl, and S. Bazin (2003), Spatial and temporal distribution of seismicity along the northern Mid-Atlantic Ridge (15°–35°N), *J. Geophys. Res.*, *108*(B3), 2167, doi:10.1029/2002JB001964.

Smith, D. K., J. R. Cann, and J. Escartin (2006), Widespread active detachment faulting and core complex formation near 13°N on the Mid-Atlantic Ridge, *Nature*, *442*, doi:10.1038/nature04950.

Smith, W. H., and D. T. Sandwell (1997), Global seafloor topography from satellite altimetry and ship depth soundings, *Science*, *227*, 1956–1962.

Spencer, J. E. (1999), Geologic continuous casting below continental and deep-sea detachment faults and at the striated extrusion of Sacsayhuaman, Peru, *Geology*, *27*, 327–330.

Staudacher, T., P. Sarda, S. H. Richardson, C. J. Allegre, I. Sagna, and L. V. Dmitriev (1989), Noble gases in basalt glasses from a Mid-Atlantic Ridge topographic high at 14 degrees N; geodynamic consequences, *Earth Planet. Sci. Lett.*, *96*, 119–133.

Sudarikov, S. M., and A. B. Roumiantsev (2000), Structure of hydrothermal plumes at the Logachev vent field, 14°45′N, Mid-Atlantic Ridge: Evidence from geochemical and geophysical data, *J. Volcanol. Geotherm. Res.*, *101*, 245–252.

Sudarikov, S. M., M. Davidov, G. Gherkashev, V. Gubenkov, O. Pivovarchuck, A. Kazachenock, and A. Mikhailov (2001), A new hydrothermal plume at 12°54.6′N, Mid-Atlantic Ridge: Initial results of the R/V/Yuzhmorgeologiya Cruise, *InterRidge News*, *10*(1), 37–40.

Thibaud, R., P. Gente, and M. Maia (1998), A systematic analysis of the Mid-Atlantic Ridge morphology and gravity between 15°N and 40°N: Constraints of the thermal structure, *J. Geophys. Res.*, *103*, 24,223–24,243.

Tivey, M. A., H. Schouten, and M. C. Kleinrock (2003), A near-bottom magnetic survey of the Mid-Atlantic Ridge axis at 26°N: Implications for the tectonic evolution of the TAG segment, *J. Geophys. Res.*, *108*(B5), 2277, doi:10.1029/2002JB001967.

Tucholke, B. E., J. Lin, and M. C. Kleinrock (1996), Mullions, megamullions, and metamorphic core complexes on the Mid-Atlantic Ridge (abstract), *Eos Trans. AGU*, *77*(46), Fall Meet. Suppl., Abstract F724.

Tucholke, B. E., J. Lin, and M. C. Kleinrock (1998), Megamullions and mullion structure defining oceanic metamorphic core complexes on the mid-Atlantic ridge, *J. Geophys. Res.*, *103*, 9857–9866.

Tucholke, B. E., K. Fujioka, T. Ishihara, G. Hirth, and M. Kinoshita (2001), Submersible study of an oceanic megamullion in the central North Atlantic, *J. Geophys. Res.*, *106*(B8), 16,145–16,161.

Tucholke, B. E., H. J. Dick, M. A. Tivey, and M. J. Cheadle (2005), Structure of Kane Megamullion, *Eos Trans. AGU*, *86*(52), Fall Meet. Suppl., Abstract T33G-01.

Uchupi, E. (1989), The tectonic style of the Atlantic Mesozoic rift system, *J. Afr. Earth Sci.*, *8*, 143–164.

Wessel, P., and W. H. F. Smith (1991), Free software helps map and display data, *Eos Trans. AGU*, *72*, 44.

Wessel, P., and W. H. F. Smith (1998), New, improved version of the Generic Mapping Tools Released, *Eos Trans. AGU*, *79*, 579.

Williams, C. M., R. A. Stephen, and D. K. Smith (2006), Hydroacoustically-recorded seismicity at the intersection of the Atlantis (30°N) and Kane (23°40′N) Transform Faults with the Mid-Atlantic Ridge, *Geochem. Geophys. Geosyst.*, *7*, Q06015, doi:10.1029/2005GC001127.